COMPARISON BETWEEN MODEL SIMULATIONS AND MEASUREMENTS OF HYPERSPECTRAL FAR-INFRARED RADIATION FROM FIRST DURING THE RHUBC-II CAMPAIGN

A Thesis

by

ELIZABETH ANN BAUGHER

Submitted to the Office of Graduate Studies of
Texas A&M University
in partial fulfillment of the requirements for the degree of

MASTER OF SCIENCE

December 2011

Major Subject: Atmospheric Sciences

COMPARISON BETWEEN MODEL SIMULATIONS AND MEASUREMENTS OF HYPERSPECTRAL FAR-INFRARED RADIATION FROM FIRST DURING THE RHUBC-II CAMPAIGN

A Thesis

by

ELIZABETH ANN BAUGHER

Submitted to the Office of Graduate Studies of
Texas A&M University
in partial fulfillment of the requirements for the degree of

MASTER OF SCIENCE

Approved by:

Co-Chairs of Committee,	Ping Yang
	Kenneth Bowman
Committee Member,	George Kattawar
Head of Department,	Kenneth Bowman

December 2011

Major Subject: Atmospheric Sciences

ABSTRACT

Comparison between Model Simulations and Measurements of Hyperspectral Far-Infrared Radiation from FIRST during the RHUBC-II Campaign. (December 2011)

Elizabeth Ann Baugher, B.S., Penn State University

Co-Chairs of Advisory Committee, Dr. Ping Yang
Dr. Kenneth Bowman

Surface downward far-infrared (far-IR) spectra were collected from NASA's Far-Infrared Spectroscopy of the Troposphere (FIRST) instrument from August to October 2009 at an altitude of 5.4 km near the summit of Cerro Toco, Chile. This region is known for its dry, cold, and dominantly clear atmosphere, which is optimal for studying the effects that water vapor and cirrus clouds have on the far-IR. Comparisons with Line-By-Line Discrete Ordinates Radiative Transfer model, LBLDIS, show that FIRST observes the very fine spectral structure in the far-IR with differences as small as +/- 0.7% for both clear-sky and cloudy-sky simulations. Clear sky model analysis demonstrated the greatest sensitivity to atmospheric conditions is between 300 and 500 cm^{-1}. The cloudy-sky simulations demonstrated that the far-IR radiation has minimal sensitivity to cloud particle effective radius, yet is very sensitive to cloud optical thickness at wavenumbers between 400 - 600 cm^{-1}. In fact, cirrus optical thickness found to be inferred from the brightness temperature differences at 250 and 559.5 cm^{-1}. Aerosols proved to reduce downwelling radiance by half that a clear-sky would emit, but had little effect on the total far-IR radiative forcing. Furthermore, these far-IR

measurements open a new window to understanding the radiative impacts of various atmospheric constituents such as water vapor and clouds, and to understanding and modeling the Earth's climate and energy budget.

DEDICATION

This is dedicated to my Dad who passed away during the time of this thesis research.

ACKNOWLEDGEMENTS

I would like to thank my committee co-chairs, Dr. Ping Yang, and Dr. Kenneth Bowman, and committee members Dr. George Kattawar, for their guidance and support throughout the course of this research. I thank them for giving me many opportunities to go to conferences, work with in-field scientists, and encourage me to continue further. I would like to thank my fellow colleagues at NASA Langley, Martin Mlynczak, Richard Cageao, David Kratz, and David Johnson for their constant updates and reviews of the manuscript. I thank Dr. Dave Turner for his time and patience with explaining the logistics and helping me with error analysis. Finally, I would like to thank Dr. Bryan Baum for his friendly and always ready help and advice.

Thanks also go to my friends and colleagues in the department faculty and staff for making my time at Texas A&M University a great experience. My research group, as well as my office mates, was essential to the success of this research. I thank my undergraduate friends and professors for continued support even after leaving Penn State. Finally, thanks to my Mom for always being there.

This study is supported by a NASA grant NNX10AL53A. The RHUBC-II campaigns were organized as a part of the U.S Department of Energy's Atmospheric Radiance Measurement (ARM) program. NASA participation was made possible thanks to NASA Radiation Sciences Program and the NASA Langley Research Center with associated subcontracts to Texas A&M University.

NOMENCLATURE

Far-IR	Far-infrared
FIRST	Far-Infrared Spectroscopy of the Troposphere
FTS	Fourier Transform Spectrometer
RHUBC-II	Radiative Heating in Underexplored Bands Campaign
TOA	Top of atmosphere
MT_CKD	Mlawer-Tobin Clough-Kneiyzes Davies
LBLRTM	Line-by-Line Radiative Transfer Model
DISORT	Discrete Dridinates Radiative Transfer
r_e	Effective Radius
τ	Optical Thickness
MLW	Mid-Latitude Winter
BTD	Brightness Temperature Difference
RF	Radiative Forcing

TABLE OF CONTENTS

Page

LIST OF FIGURES

Page

Page

LIST OF TABLES

1. INTRODUCTION: THE IMPORTANCE OF RESEARCH

The spectral region between 15 μm and 100 μm (667 – 100 cm^{-1}) is referred to as the far-infrared (far-IR) portion of the spectrum. Far-IR radiation is an important component of the radiation budget in the earth-atmosphere system and accounts for approximately 50% of the top of atmosphere (TOA) outgoing longwave radiation [e.g., *Collins and Mlynczak*, 2001]. One of the key features in the far-IR spectral range is its characterization of transitions between pure rotational and low vibrational energy states. The pure rotational band associated with water vapor largely affects this spectral region in which it acts as one of the principal greenhouse gases, absorbing a significant fraction of the infrared radiation emitted by the atmosphere and the earth's surface. Due to the strength of the water vapor band, the lower atmosphere is essentially opaque in the far-IR spectrum for ground-based observations, while the upper troposphere and stratosphere become partially transparent. These associated complications have caused the spectral characteristics and information content of the far-IR region to not be studied extensively. The radiative processes in these water vapor absorption bands are critical to understanding the radiative balance of the tropopause layer and lower stratosphere.

Additionally, far-IR radiation can be modulated by the presence of cirrus clouds in the upper troposphere. These clouds pose a significant challenge for in situ measurements because of their high altitudes and optically thin nature [*Liou*, 1986].

This thesis follows the style of *Journal of Geophysical Research-Atmospheres.*

Previous studies of cirrus clouds show that they may radiatively cool or heat the upper atmosphere in the thermal infrared wavelengths depending on altitude and geometrical and microphysical features [*Harries et al.,* 2008]. The single scattering properties of cloud particles are determined by the complex index of refraction ($m = m_r + im_i$), the particle size distribution, and the shape of the particles. Figure 1 displays both the real and imaginary parts of the refractive index of ice based on the data compiled by Warren [1984], showing that ice crystals are strongly absorptive in the far-IR. The minimum in the imaginary part of the refractive index is located at 410 cm^{-1}, and corresponds to the strongest scattering effect, while, the minimum in the real part of the refractive at 250 cm^{-1}, corresponds to an area of very low extinction efficiency. These ice properties offer the potential to determine the optical properties of cirrus clouds. Most recent studies include the scattering database and absorption properties of ice clouds for mid and far infrared determined by observation [*Yang et al.,* 2005; *Baum et al*, 2007].

The Radiative Heating in Underexplored Bands Campaigns (RHUBC) were designed to improve our understanding of radiative processes in the middle and upper troposphere and lower stratosphere [*Turner and Mlawer,* 2010]. The campaigns are part of the Atmospheric Radiation Measurement (ARM) program, which, was established by the U.S. Department of Energy to improve aspects of climate simulations related to atmospheric radiative transfer. In particular, these experiments will help to improve the accuracy of line-by-line radiative transfer models by developing better approximations of the water vapor continuum absorption in the far-IR and reducing the number of

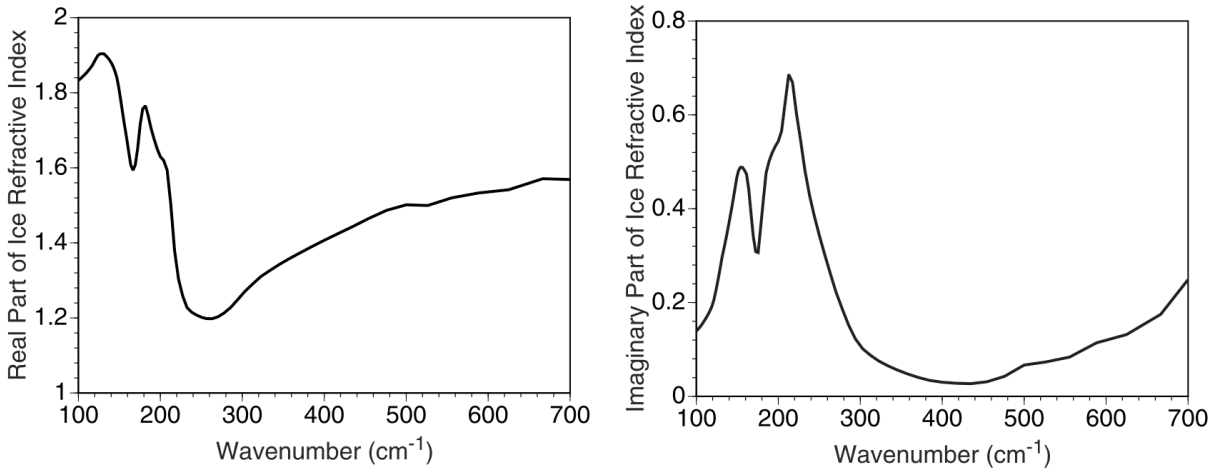

Figure 1: The variation of refractive index of ice in the far-IR region (data from [*Warren*, 1984]).

spectroscopic parameters used to model water vapor absorption in the far-IR. In this multi-phase campaign, locations were chosen for their extreme dryness, which enabled direct observation of the full spectral development of the far-IR, which is not possible in other environments. RHUBC-I ran from February to March 2007 in Barrow Alaska, and had successful results [*Turner et al*., 2010; *Delamere et al*., 2010]. The usage of interferometer AERI [*Turner et al*., 2003; 2010; *Turner*, 2005] and spectrometer TAFTS [*Cox et al.,* 2010] during this campaign present some of the most promising and recent findings. RHUBC-I had three very important contributions which include: (1) the three, 183-GHz (6.11 cm^{-1}) millimeter radiometers, agreed very well with each other (2) the refinement of the 183.3-GHz water vapor line and (3) improvement to the line-by-line radiative transfer models in the 16-25 μm (625 – 400 cm^{-1}) band [*Turner and Mlawer*, 2010].

As an extension to continue to improve our understanding of the dominant radiative processes in the troposphere and stratosphere, the RHUBC-II field experiment was run from August to October 2009 at Cerro Toco, Chile. The novel Far-Infrared Spectroscopy of the Troposphere (FIRST) instrument developed by NASA [*Mlynczak et al.,* 2006], a Michelson interferometer, provides unprecedented measurements of far-IR downwelling radiation. The FIRST Fourier Transform Spectrometer (FTS) measures in the far-IR portion of the earth's emission spectrum, offering a unique opportunity to study atmospheric radiation and climate, cirrus clouds, and water vapor in the upper troposphere. Far-IR measurements are crucial to understanding the Earth's climate and will radically improve our ability to model and predict the future of the Earth's energy budget.

Finally, in addition to the ice cloud studies, dust particles are also analyzed for their effect on the far-IR radiation. Aerosols play an important role in Earth's climate system through both direct and indirect effects on the energy budget and hydrological cycle (*Zhaokai et al*., 2010). The Earth-atmosphere system has both natural aerosols (pollen, bacteria) and anthropogenic sources (products of combustion, smoke, ashes, dusts). Due to the variety of shapes, sizes and forms, the factors that determine how aerosol radiative forcing may behave are very hard to understand. Numerous methods have been used in attempt to understand aerosol optical properties and radiative influences through model simulations and satellite-derived measurements. However the majority of these techniques have only included the visible and infrared regions of the

electromagnetic spectrum, leaving the effect of aerosols in the far-infrared (IR) region a big uncertainty.

The main objectives of this work is to (1) compare and validate the FIRST measurements and simulations (2) analyze the measurements to understand sensitivity of the far-IR spectrum to atmospheric constitutes and properties and (3) explore the information content of ice clouds and dust clouds to develop ice cloud retrieving algorithms and aerosol properties. Therefore this work is organized in the following format: Section 2 presents the data used as well as the FIRST instruments description. Section 3 provides an overview of methods and models used to determine simulations. Section 4 presents results in order of clear-sky simulations, cloudy-sky simulations, and cloud-property sensitivity study simulations. Section 5 discusses findings on aerosols in the far-IR and finally, section 6 summarizes the main findings of this work.

2. DATA

2.1 FIRST Instrument

The FIRST instrument is designed to cover the spectral region from 10 to 100μm and provides a spectral resolution of 0.643 wavenumber (unapodized). Table 1 lists some characteristic parameters of the FIRST instrument used. FIRST incorporates a high-throughput (0.47 cm^2 steradian) interferometer to adequately fill a 10x10 (100-element) focal-plane sensor and a single broad bandpass beamsplitter (germanium on polypropylene) to pass the entire spectral interval and scan in periods as short as 1.4

Table 1: The FIRST Fourier Transform Spectrometer characteristics for far-IR measurements. Note: spectral range is for analyzed dataset and resolution is the operating resolution.

Characteristic	**FIRST**
Instrument Type	2-port Plane-Mirror FTS
Optical Throughput	0.47 cm^2 ster
Spectral Range	80 – 800 cm^{-1}
Resolution (unapodized)	0.643 cm^{-1}
Detectors	10 Si bolometers
Beamsplitter	Ge on polypropylene
Scan time (double-sided interferogram)	8.5 sec
Sky Integration	6 min.
Calib. Blackbodies	46 and 12 C
Period between Calibrations	35 min.
Lab Calibration Uncertainity	< 1K

seconds. The FIRST FTS system includes three view ports: one for viewing the atmosphere, and two for viewing calibration sources and is displayed in Figure 2. Light enters through the scene select motor, reflects through the interferometer cube and finally reaches the detector dewar, where measurements are stored. The scene selection mirror rotates depending on the three measuring locations (space view, ground based, or flight blackbody) and scans over an optical path of +/- 0.8 cm. A thin polypropylene window isolates the scene select mirror from the interferometer dewar. The FIRST beamsplitter uses a multi-layer beam splitter with germanium and polypropylene. This material is used because it has relatively few absorption features in the measured wave spectrum. The FTS and aft optics are cooled to approximately 180K by liquid nitrogen, and the detectors are cooled to 4.2K, while the rest of the instrument is at ambient temperature.

Calibrations for FIRST include both radiometric and spectral uncertainties. For radiometric corrections, FIRST viewed two different calibration blackbodies; one at ambient temperatures ranging from 277 to 285K and one maintained at higher temperatures between 310 and 319K.

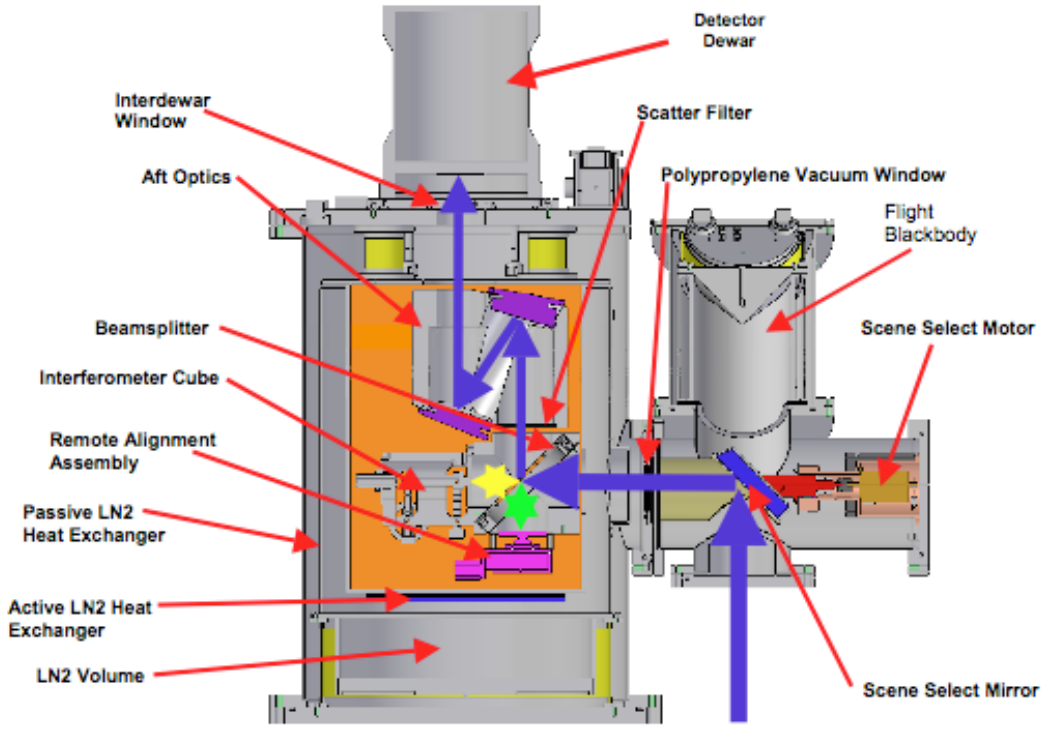

Figure 2: The three optical modules in the FIRST FTS system.

The temperatures were stable to a couple degrees over the course of the day and were stable to much better than that over the course of an individual calibration scan. These warm and cold sources were taken for different configurations and then used to correct interferograms for small non-linearity phase offsets. Additionally, spectral uncertainties were corrected for off-axis frequency shifts in the scene select mirror and

summed multiple detectors for increased precision. Further detailed information on the FIRST instrument can be found in *Mlynczak et al*. [2005, 2006].

2.2 FIRST Data

Surface downwelling far-IR radiation measurements were collected from August through October 2009 in Cerro Toco, Chile (23°S, 67.8°W) using the FIRST Fourier Transform Spectrometer [*Mlynczak et al.,* 2006] as part of the RHUBC-II campaign [*Turner and Mlawer,* 2010]. Located in the Atacama Desert, the summit of Cerro Toco is at 5.4 km above sea level in the Andes Mountains and is known to be one of the driest and clearest locations in the world because of the region being in the rain shadow between mountain ranges; the walker circulation (air descends); and the cold ocean water off the coast (coastal inversion) [*Turner and Mlawer*, 2010]. The campaign time period was chosen to correspond to the lowest precipitable water vapor column amounts (PWV) during the year, averaging 0.3 to 1.5 mm. The water vapor abundances at this site are similar to those seen in the mid-to-upper troposphere, a rare occurrence at a surface-based site. With these low PWV values, the atmosphere becomes semi-transparent in the far-IR, which allows for the spectral structure of water vapor absorption to be observed.

In addition to the ground-based downwelling radiation measurements, Vaisala RS92 sondes were launched at 1-hour intervals from the Cerro Toco site and recorded pressure, temperature, and relative humidity, as a function of altitude. PWV measurements were retrieved using a 183-GHz (6.11 cm^{-1}) G-band vapor radiometer, which can detect the strong microwave water vapor absorption lines [*Turner and*

Mlawer, 2010] and proved to be accurate in the RHUBC-I experiments. Relative humidity values were scaled to the measured PWV to remove sonde biases, which can occur in the upper and lower troposphere, as described in *Miloshevich et al.* [2009]. The atmospheric profiles used in these analyses are the RHUBC-II Chile sonde files version 2.0.

The FIRST measurements analyzed in this study include five dates from September and October 2009 that are representative of both clear and cloudy sky conditions. For comparison purposes, days were divided into moist and dry days based on measured relative humidity values and PWV. Table 2 lists the dates used in this study with respective atmospheric variables. 10 September, 13 September and 5 October, represent dry days whereas 1 October and 3 October represent moist days. The timing of both the FIRST measurements and the sonde profiles were matched as closely as possible.

Table 2: Summary of dates and time stamps used in this study with respective variables and notes on moisture categorization and cloud condition took during experiment. Note that type of cloud is not determined. 1 October 2009 at 17:40z is the only date used for cloudy-sky simulations.

Date/Launch Time	Sfc Temp (K)	RH (%)	PWV (mm)	FIRST Notes	Satellite Determination
10 September 2009 15:29z	264	18.4	0.5	Dry. Clear	Clear
13 September 2009 13:44z	268	6.1	0.3	Very dry. Clear	Clear
1 October 2009 15:26z	268	25.9	1.0	Moist day. Clear	Clear
1 October 2009 17:40z	270	31.5	1.2	Moist. Cloud noted	Cloudy
3 October 2009 17:30z	277.6	8.6	0.95	Moist. Warmest Day.Cirrus Near	Clear
5 October 2009 15:55z	273.3	6.6	0.6	Dry. Thin Cirrus Noted	Clear

3. METHODS

3.1 Models

Line-by-line radiative transfer (LBLRTM) models can be used to analyze the far-IR hyperspectral characteristics [*Clough et al.,* 1992; 1994; *Cageao et al*., 2010]. LBLRTMv11.7 uses the RHUBC-II radiosonde atmospheric profiles to calculate the gaseous optical depths at 40 linearly spaced layers between the minimum and maximum altitude by using the line parameter database (aer_v_2.4) to provide atmospheric line positions, strengths and shapes [*Rothman et al*., 2005]. This line parameter database includes updates to the carbon dioxide line intensities between 597-2500 cm^{-1}, as well as water vapor line shifts and temperature dependencies for lines from 436-2396 cm^{-1}. Information on concentrations of other atmospheric gases active in the region of interest were based on the standard mid-latitude winter model, which is built into the LBLRTM model. The model also incorporates a continuum absorption model (MT_CKDv2.5) for the "continuum absorption" of overlapping wings of water vapor absorption features [*Clough et al.* 2005]. The water vapor continuum used includes the most recent updates to far-infrared wavenumbers made in version 2.4 by the RHUBC-I results. This water vapor continuum model is very important to the accuracy of LBLRTM because of the assumed absorption parameters (line shapes, strengths and position) stored in the absorption line database. The evaluation of this water vapor continuum model in the far-IR is a high priority of the RHUBC campaigns.

As a flexible model that computes radiance for scattering atmospheres and has primarily been used in the infrared [*Turner et al*., 2003; *Cox et al.,* 2010], LBLDIS

(v2.1) [*Turner*, 2005], is a combination of LBLRTM and the Discrete Ordinates Radiative Transfer (DISORT) method [*Stamnes et al.,* 1988]. This model can account for a vertically inhomogeneous atmosphere consisting of a number of vertical layers including cloud layers. It is able to compute the radiance emitted by the atmosphere at any altitude, viewing angle, and arbitrary spectral resolution. The model reads the LBLRTM calculated optical depths, as well as the atmospheric temperature profiles and assigns each cloud layer (if any) the bulk single-scattering properties [*Baran et al*., 2005; *Baum et al.,* 2007] including the single-scattering albedo, phase function and cloud optical thickness.

3.2 Clear-Sky Modeling

For clear-sky simulations the surface temperatures reported in Table 2 are used for the input temperature in the LBLDIS model. Additional inputs into the LBLDIS model include wavenumber start and end (100-700 cm^{-1}), resolution (to match the FIRST measurements, 0.643 cm^{-1}), zenith angle (180 degrees (downwelling)), solar zenith angle (60 degrees), and relative azimuth angle (30 degrees). Angles are subject to change based on date and time, however these average angles are representative of a typical downwelling measured scene with nadir as the point of view. Furthermore, surface spectral emissivity lines can be input; however, findings show that the far-IR has a relatively constant surface emissivity across the globe close to one [*Seemann et al*., 2008]. The simulated radiance values were convolved with an apodizing von Hann function [E.W.Weisstein. "Hanning Function" available from MathWorld--A Wolfram Web Resource. (http://mathworld.wolfram.com/HanningFunction.html)] to smooth the

instrument sinc function for comparison with the similarly convolved measured spectra of the instrument.

3.3 Cloudy-Sky Modeling

For cloudy-sky simulations the same above inputs were used with the addition of certain cloud parameters such as number of cloud layers, cloud height, reference wavenumber, effective radius, and optical thickness. A scattering database of the single-scattering properties of cloud particles, including the single-scattering albedo, extinction coefficient, and phase function, is used to define the optical properties of a cloud. Historically, cloud particles have been treated as spheres and the scattering properties of these particles can be computed using the Lorentz-Mie theory. However, ice clouds are almost exclusively composed of non-spherical ice crystals. In previous work, various ice crystal habits, or shapes, have been observed in cirrus clouds, including hexagonal columns and plates, bullet rosettes, and aggregates [*Heymsfield et al.,* 2002]. *Lee et al.* [2003] shows that the effect of the sharp edges of pristine ice crystals may not be important at far-IR wavelengths because of the strong absorption of ice in this spectral region. For the purposes of the effective radius (r_e) sizes studied in this work, solid columns are used to represent the ice crystals, which typically have a mean r_e = 38.46 μm [*Key*, 2002]. In the present study the single-scattering properties of solid hexagonal ice columns are taken from a scattering database [*Yang et al.,* 2005] that was developed by using a composite method based on the finite-difference time domain (FDTD) method and an improved geometrical-optics method (IGOM) [*Yang and Liou*, 1996a; 1996b] for nonspherical particles and the Lorentz–Mie theory [*Wiscombe*, 1980] for

equivalent spheres. The single-scattering properties are integrated over a gamma size distribution for effective particle sizes ranging from 1 to 1000 μm, for the entire far-IR, and infrared regions. These properties were derived with sigma = 0.1, which indicates the spread of the gamma function used. It should be noted that the effective radius utilized in this work is equal to half the effective particle size and is proportional to the ratio of the volume to the projected area of the size distribution of the crystals defined by [*Foot,* 1988; *Baum et al.* 2005; and references cited therein]:

$$r_e = \frac{3}{4}\frac{V_{tot}}{A_{tot}} \qquad (1)$$

Additionally, the optical thickness defined in this work is calculated using the cloud geometrical thickness (z) and the volume extinction coefficient (β_{ext}), which changes with changing effective radius and can be found in the calculated bulk scattering particle database.

$$\tau = z * \beta_{ext} \qquad (2)$$

The ice particle database thus contains the wavelength range covered, effective radius, extinction, scattering and absorption cross section and efficiency, single scattering albedo, asymmetry parameter, projected area, volume and the scattering phase function at 498 scattering angles from 0° to 180° for solid column crystals.

Cloud properties were not measured during RHUBC-II. A micro-pulse lidar for the purpose of measuring cloud properties was on site but did not function properly during the campaign. Therefore, sky condition (clear or cloudy) is noted in Table 2 by

using a combination of satellite data from GOES-14, CALIPSO and MODIS-Terra Cloud Products. Note that cloud type is not available, but for 1 October 2009, 17z a thin-cirrus is assumed for the purposes of this study. Unfortunately, the retrieval of cloud properties (i.e. optical thickness and effective radius) from cirrus detection (when visible optical thicknesses are <0.3) is often skewed in satellite measurements because of the inability of the retrieval algorithms to detect the scattering and absorption properties of small ice crystals [*Meyer et al.,* 2004; *Ackerman et al.,* 2008]. Following previous analysis, [*Meyer et al*., 2004, *Yang et al.*, 2003, *Cox et al*., 2010] the optical thickness of a cirrus cloud is in reference to its value at a visible wavelength. *McFarquhar et al.* [1999] found that the most frequent combinations of thin cirrus include an ice crystal habit distribution with effective diameter D_e = 24 μm and optical thickness $\tau \leq 0.3$. On the other hand, *Baum et al.* 2007, found a 100% solid column distribution with D_e=92 μm fit slightly thicker cirrus ($\tau \geq 0.4$–0.5). Therefore, by using a combination of these findings, the following basic thin cirrus assumptions were used to start evaluating cloud properties: optical thickness, $\tau = 0.2$ and effective radius, $r_e = 10.0$ μm , where $r_e = \frac{1}{2}D_e$. For simplicity of modeling, cloud height input was obtained from the satellite data and for the cloudy simulation on 1 October 2009 at 17:40z, height is equal to 6.13 km.

3.4 Aerosol Modeling

In order to study the effects of aerosols in the far-IR region, the optical properties of aerosols must be determined. Due to aerosols nature to be hygroscopic, aerosol optical single scattering properties (including extinction, scattering and absorption coefficients, single scattering albedo, and asymmetry parameter) are all wavelength

dependent and must be calculated for each wavenumber. To simulate aerosols in the far-IR, a combination of line-by-line radiative transfer model (LBLRTM v11.7), discrete ordinates radiative transfer model (DISORTv2.1), Zhaokai derived bulk scattering aerosols database, and the FIRST simultaneously acquired far-IR downwelling radiances are used (*Clough et al.,* 2005; *Stamnes et al.*, 1988; *Zhaokai et. al*., 2010; *Mlynczak et al.,* 2005). Again, the atmospheric profiles are used in LBLRTM to calculate optical depths at 40 different layers from the surface to the top of atmosphere (5.4 km to 17.4 km). Each optical depth layer is then interpolated from high resolution to moderate resolution in order to account for the different spectral ranges in each layer. Next, the exact optical depth calculations are use to build the bulk-scattering database. *Zhaokai et al.,* 2010 provides a user-friendly single scattering database for tri-axial ellipsoidal mineral dust aerosols, which can be used to calculate bulk scattering properties based on two aspect ratios, complex refractive indices and a size parameter. The database is prepared using a look up table for the complex refractive indices of dust taken from *Levoni et al*., (1997). Because values have not been calculated for wavelengths > 40 μm, the values at 40 μm are assumed for m_r and m_i. In these simulations the database used was created with $m_r = 1.9$, $m_i = 0.5$ (highly absorptive), a/c = 0.52, b/c = 0.75, and a lognormal size distribution. This database is then used in DISORT to simulate downwelling aerosols in the far-IR. For these model simulations, the extinction coefficient (visible) is determined from the optical depths and is set to 2.30674. Calculations of simulated data are finally interpolated to the FIRST resolution for comparison.

4. RESULTS

4.1 Clear-Sky Simulation

Under clear-sky simulations, the LBLDIS model shows strong agreement with the FIRST measurements, follows the general measured trend given by the FIRST instrument, and mimics water vapor continuum absorption across the spectrum, as demonstrated in Figure 3. Line structure shown in Figure 3 below 500 cm^{-1} is due mainly to the pure rotational structure of water vapor. The spike at band 667cm^{-1} is due to instrument internal CO_2 absorption at higher temperature in the optical path. Figure 4 shows that the peak-to-peak differences between the clear sky simulation and FIRST measurements for 10 September 2009 at 15:29 are quite small and do not exceed +/- 0.7 %, except at the CO_2 absorption band. The differences between 600 and 700 cm^{-1} are due to a combination of errors in the models CO_2 band absorption parameters and the near surface temperature specification, (FIRST trailer was warmer than outside air). This has not been corrected for and is an active area of research. The difference calculations for each of the other studied dates displayed similar characteristics.

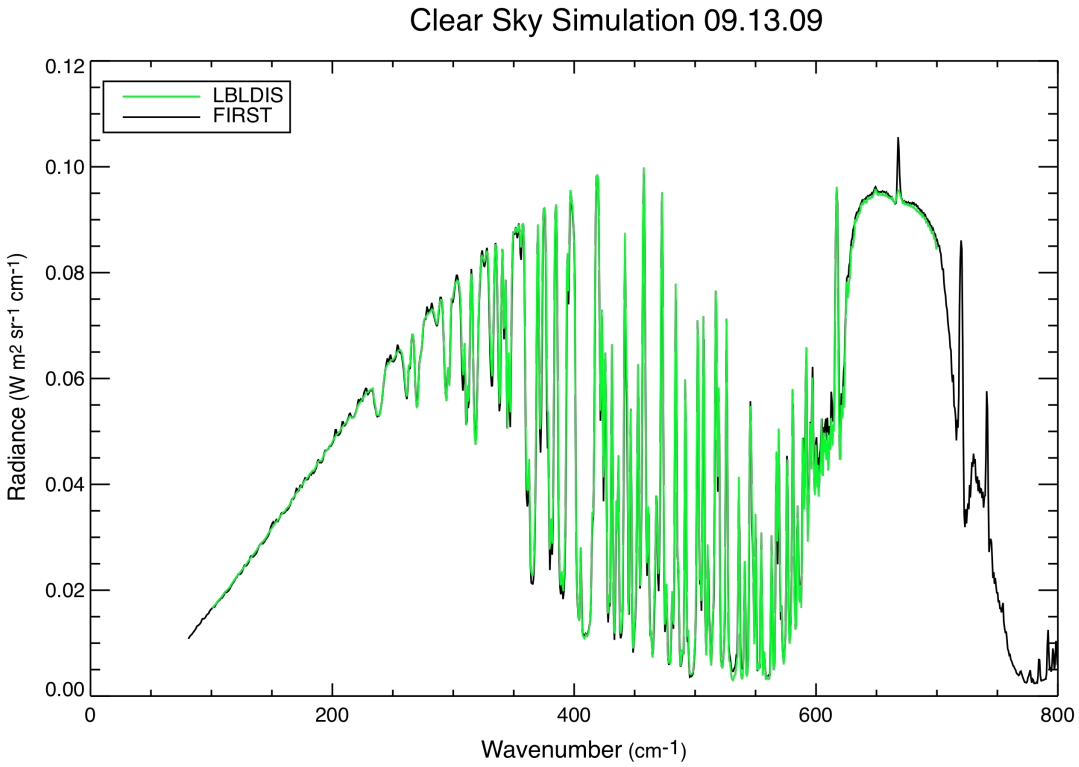

Figure 3: FIRST downwelling radiance measurements overlaid with the LBLDIS model of a clear sky simulation for 10 September 2009 at 15:29z.

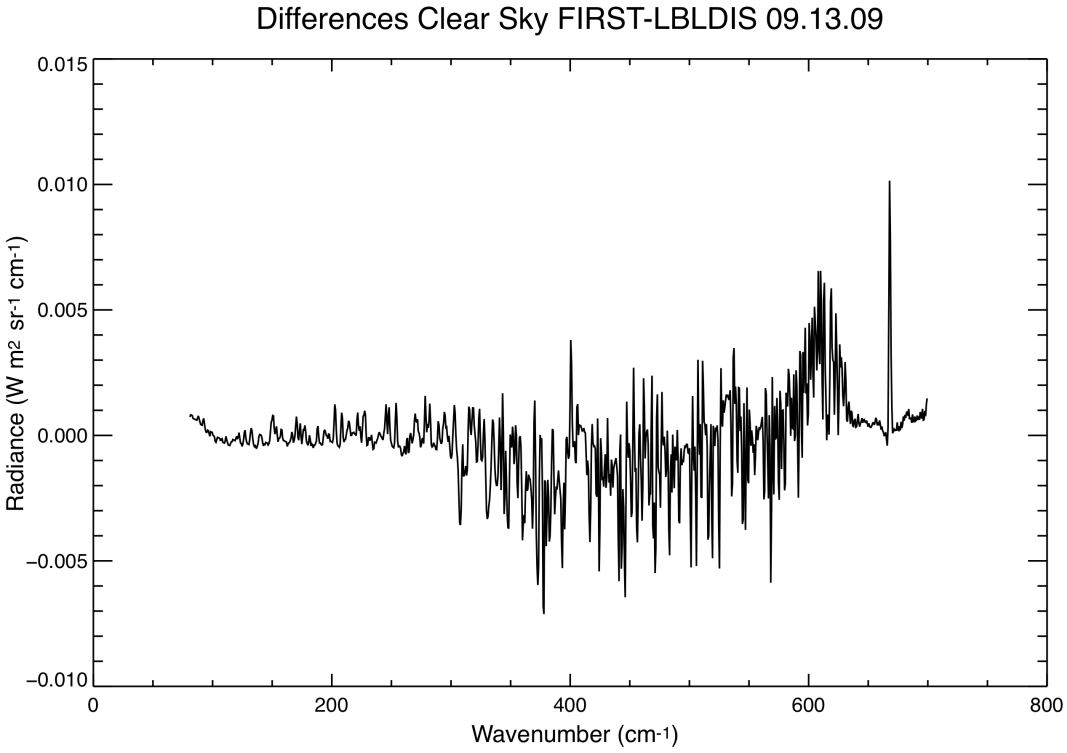

Figure 4: Example showing very small differences of the radiance at each wavenumber between the model and measured spectral downwelling radiances.

Due to similar difference spectrums for each of the days studied, it is interesting to look at the effects that moisture differences may have on these calculations. In order to do so, the dates were compared respectively based on dry and moist categorization determined by PWV. As mentioned in the data section Table 2, 13 September 2009 is an example of a dry date and 3 October 2009 is an example of moist date. Before comparison, it is useful to see what the water vapor profiles looked like for each date. Figure 5 compares the Cerro Toco water vapor spectrums from each day, with the addition of a mid-latitude winter (MLW) profile for reference. Note that water vapor

amounts are very dry in the lower troposphere and become even drier once entering the upper troposphere (altitude > 12 km). Previous literature has also shown that this region in the far-IR is linked to the greatest atmospheric cooling rates in the middle and upper troposphere [*Clough et al.,* 1992].

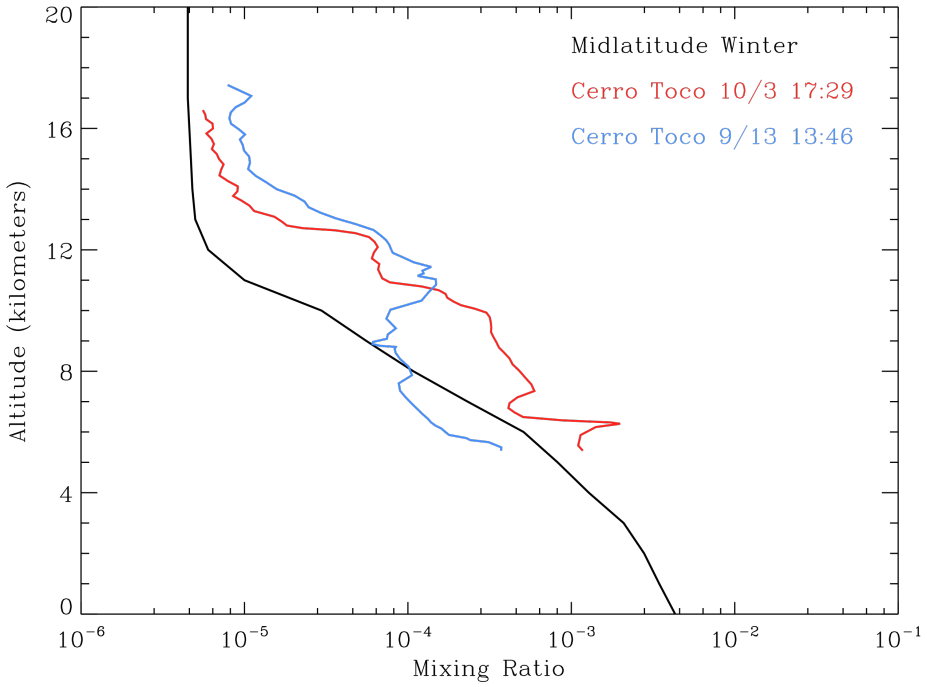

Figure 5**:** Comparison between MLW water vapor profile and simultaneously acquired Cerro Toco water vapor profiles from the respective dates. 13 September represents a dry day and 3 October represents a moist day.

Despite water vapor differences in the lower troposphere between these two dates, it should be emphasized than when using the simultaneously acquired water vapor, the model still shows very good agreement. Figure 6 displays the spectrum between 300-500 cm^{-1} for both the moist day (3 October 2009) and the dry days (13 September 2009) model simulation and observed simulation. This region was selected because the mean error was the greatest for this spectral region. Figure 7 displays the difference spectrum between the clear sky simulation and the observed measurements for both the dry and moist cases. The differences are small (+/- 0.7%) and the greatest errors for each water vapor case peak at the same wavenumber bands, illustrating the models sensitivity to the water vapor differences.

The differences seen may be more than just atmospheric condition related and may also be affected by the water vapor continuum used in the model. The continuum used (MT_CKD v 2.4) in this study includes the most recent far-IR water vapor updates to bands 410, 477, 497, 533, and 560 cm^{-1} [*Delamere et al*., 2010].

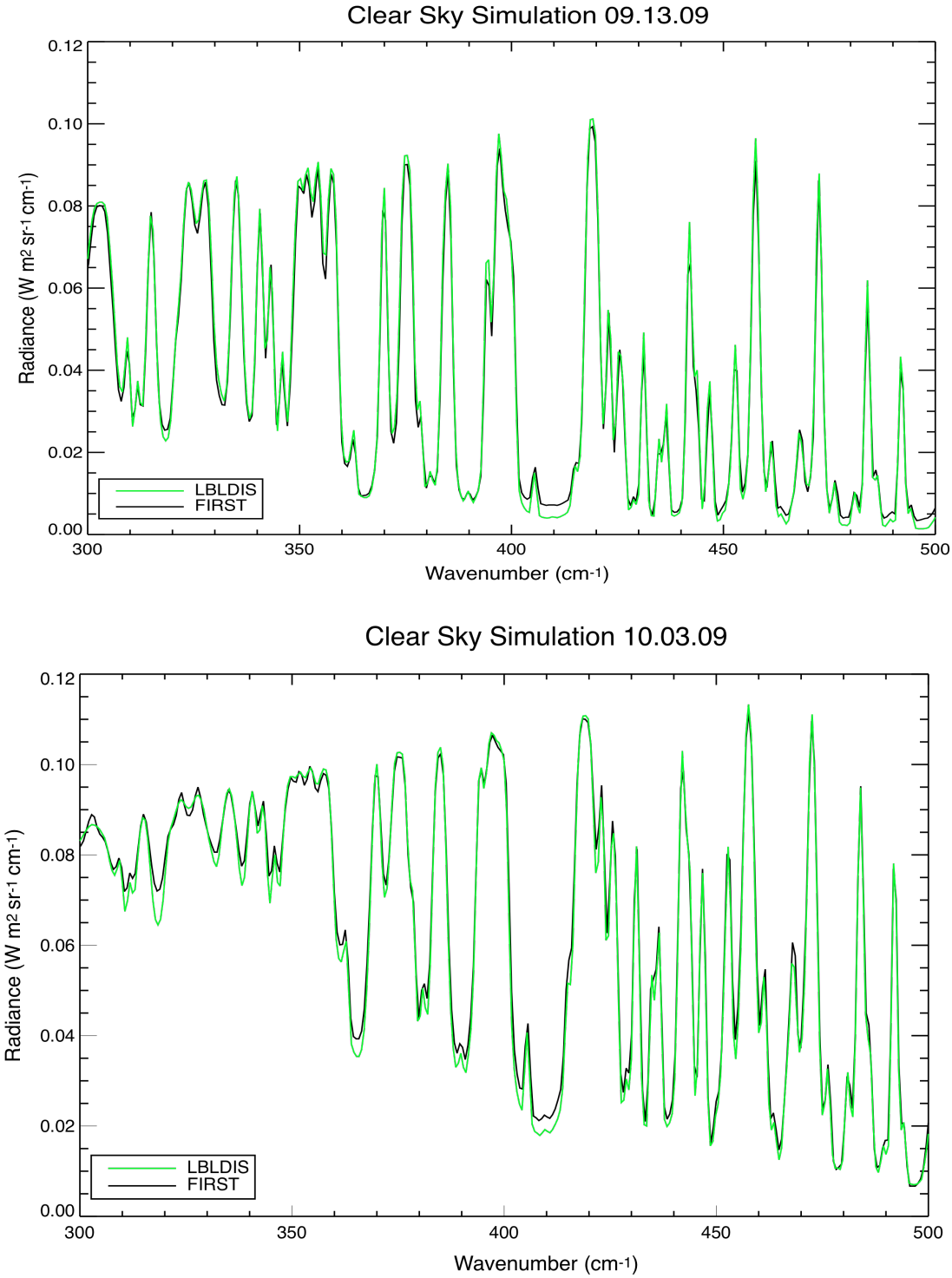

Figure 6: Comparison between dry day, 13 September, and moist day, 3 October, for a clear sky simulation. Using the simultaneously acquired water vapor profile for both wet and dry days, the model shows very good agreement for this interval.

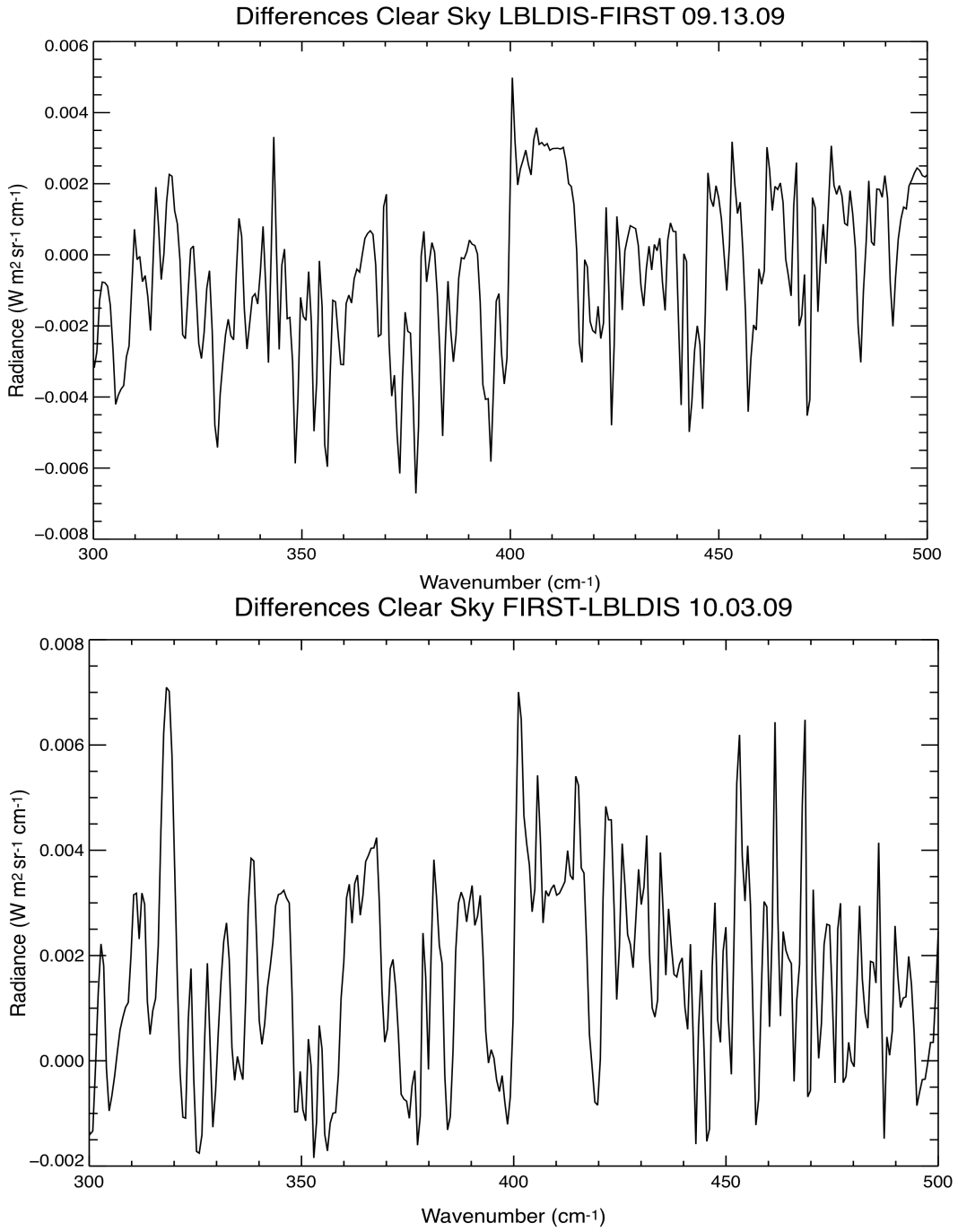

Figure 7: The differences between the FIRST simultaneously acquired measurements and the clear-sky model simulations for each respective date. Differences are relatively small, with peak differences the same for both the dry and moist case. Updates to additional far-IR water vapor bands are imperative for future studies.

Updates to additional far-IR water vapor bands are imperative for future studies. In order to understand problematic water vapor absorption bands used in the continuum, the total differences between the moist and dry day's differences are calculated to highlight particularly strong absorption bands. This "total" difference consists of first calculating the differences of the simulation and actual (for each separate water vapor case), in order to account for model biases. Then, the total differences of these calculations are computed to account for both model sensitivity and water vapor sensitivity. Figure 8a displays the moist and dry, clear-sky simulations for comparison. Figure 8b displays the total calculated differences between the dry case and the moist case simulations. The greatest biases seen in figure 8b are suggestive of bands that may need improvements in the future model of the water vapor continuum. Improvements made to the water vapor continuum, particularly at these wavenumbers, may be a method toward achieving good model agreement [*Clough et al*., 1992; 2005].

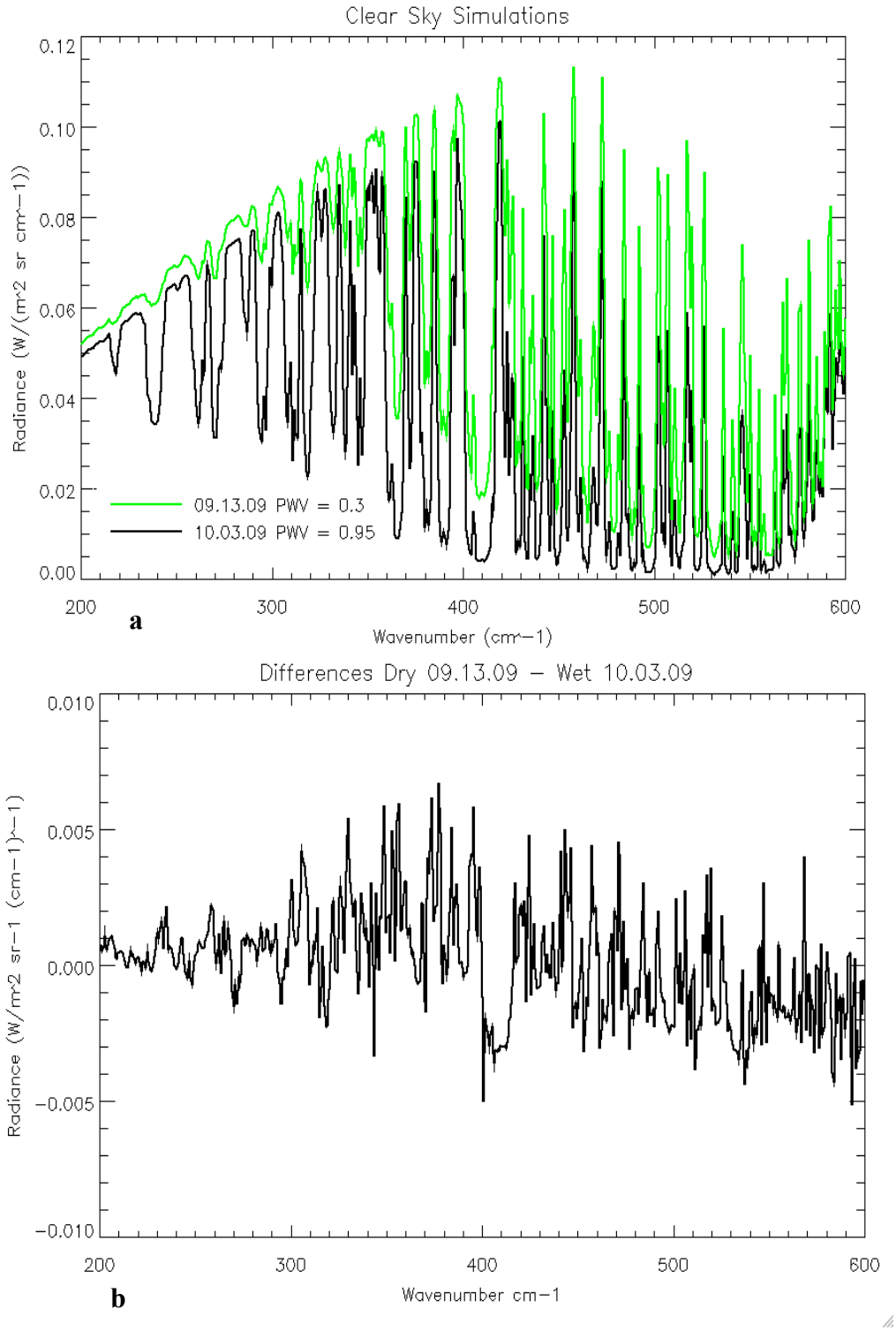

Figure 8: a.) Comparison of clear-sky model simulations for both dry and moist cases. b.) Total differences between dry and moist clear-sky simulation highlight bands that may need special consideration and updates in the water vapor continuum.

4.2 Cloudy-Sky Simulations

Although the significant role of ice clouds in the climate system has long been recognized [*Liou,* 1986; *Lynch et al*., 2002], a complete understanding of this role has not yet been achieved. Bulk radiative studies of cirrus clouds show that cirrus clouds may radiatively heat or cool the upper atmosphere at infrared wavelengths depending upon the height, thickness and microphysical size of the clouds [*Fleming et al*., 1974; *Mlynczak et al*., 2006]. To understand the effects of cirrus clouds in the far-IR, the cloud microphysical properties, effective radius (r_e) and optical thickness (τ), were varied for the cloudy case 1 October 2009 at 17:40z.

In order to analyze the effects that thin cirrus clouds would have in the far-IR, the cloud microphysical properties are input into the LBLDIS model. Model inputs for the cloud are as discussed in the methods sections ($\tau = 0.2$, $r_e = 10.0$ μm, cloud height = 6.13 km, solid column ice scattering database). Results show that with these basic thin cirrus cloud assumptions, there are some differences particularly in the spectrum at wavenumbers greater than 400 cm^{-1}. Figure 9a shows the difference comparison between the model simulation with cloud parameters to the FIRST measurements, and the model simulation with clear sky properties to the FIRST measurements. It can be observed that when there is a thin cirrus cloud present, the model is sensitive to the cloud properties particularly between wavenumbers 400-600 cm^{-1}. Figure 9b shows the difference between the clear sky and cloudy sky simulation. It is apparent that the cloud properties have the greatest effects on the far-IRs larger wavenumbers (>400 cm^{-1}). This is coincidently the region of the strongest scattering for ice in the far-IR.

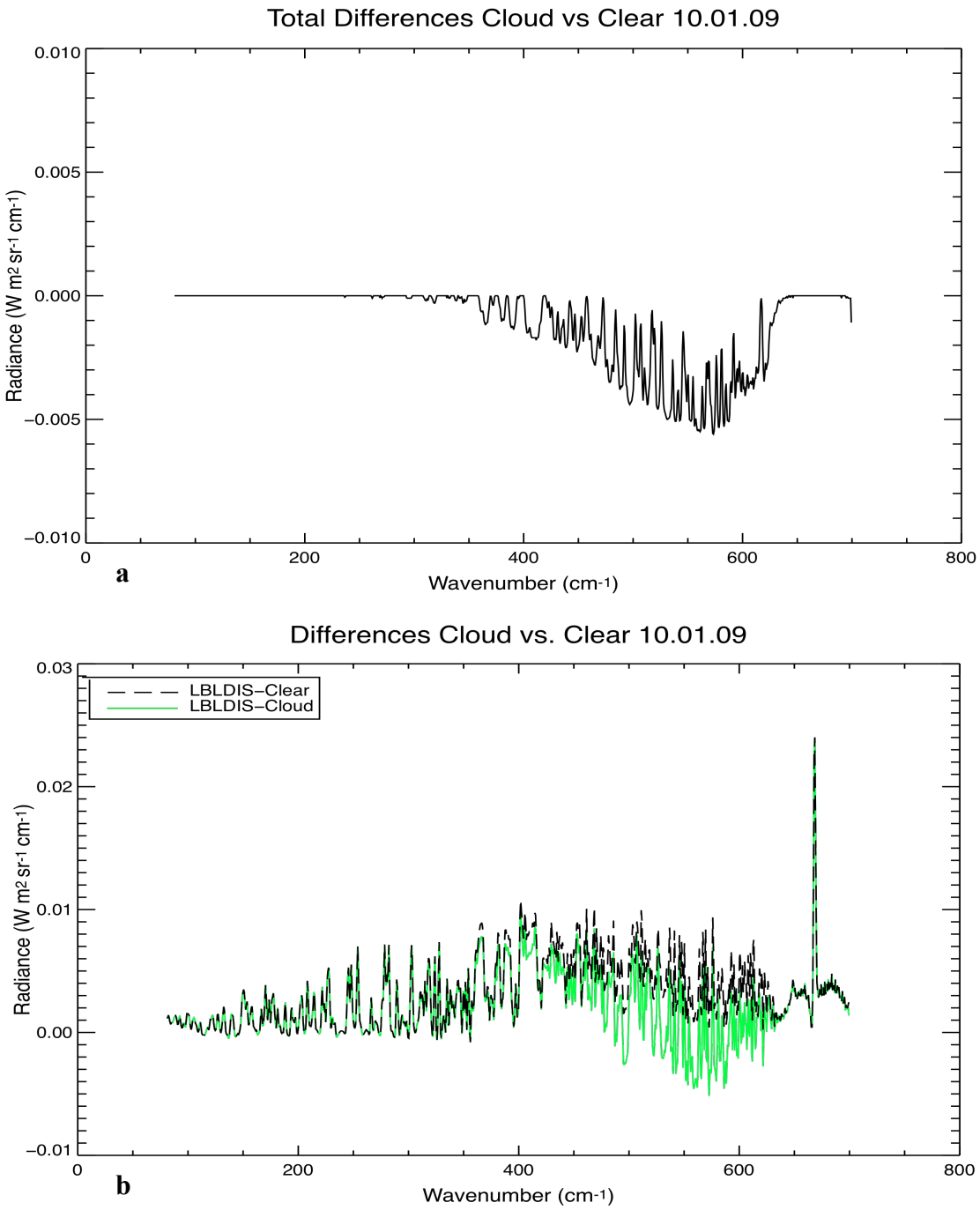

Figure 9: a.) Comparison of the differences between the clear sky simulation and the observed measurements and the cloudy sky simulation with the observed measurements. b.) The sum of the clear sky simulation differences and cloudy sky simulation differences. The cloudy sky model simulation is most sensitive at wavenumbers between 400 - 600 cm^{-1}.

4.2.1 Effective Radius Study

Since the actual cloud optical thickness and effective radius are not known for this cloudy day, it is useful to test other size ranges for these microphysical properties. In order to analyze the effect that particle size is having on the model, increments of effective radius = 10μm are applied. Results show that by increasing the radius, differences between model simulations are very small. Figure 10a shows a comparison between r_e = 10.0 μm and r_e = 50.0 μm for a cloudy sky simulation on 1 October 2009, 17z, with the same cloud properties as before. Figure 10b emphasizes that minimal differences are seen across the spectrum for increasing effective radii, with slight sensitivity at wavenumbers > 400 cm^{-1}. This particular spectral structure mimics absorption line features from water vapors rotational structure on the far-IR. Because these bands have not been fully studied, it raises the question as to whether the water vapor continuum is compensating for the inadequacies in the model with the cloud, or if it is really the cloud property effective radius. *Delamere et al*., 2010 discusses that the most recent updates to the far-IR part of the water vapor continuum are in the MT_CKD 2.4 model, which resulted in significant radiance model improvements between 400 and 625 cm^{-1}, particularly at wavenumbers 410, 477, 497, 533 and 560 cm^{-1}. Though this model proved adamant, the continuum has not had far-IR improvements since 2009, and measurements from campaigns such as these can help to distinguish where improvements may be needed.

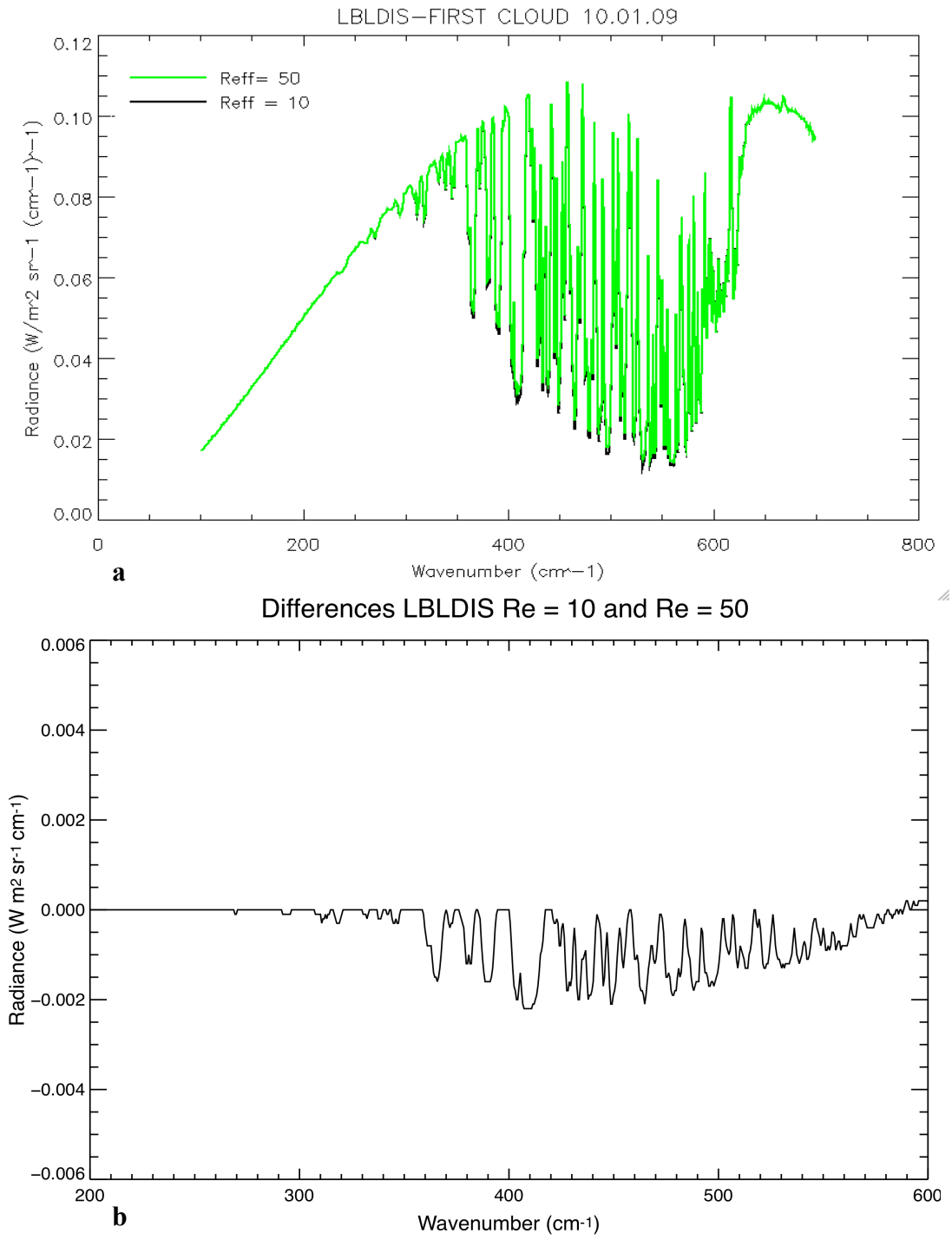

Figure 10: a.) Cloudy-sky simulation with basic thin cirrus cloud parameters for different effective radius r_e = 10.0 µm and r_e = 50.0 µm. b.) Differences between cloud simulation with r_e = 10.0 µm and r_e = 50.0 µm are very small. The downwelling radiance in the far-IR is only slightly sensitive to the particles effective radius at wavenumbers > 400 cm^{-1}.

To distinguish if the water vapor continuum is the main culprit to these differences, the same analysis was done for the very dry, cloud free date 13 September 2009, 13:44z, using the same cloud properties described above for both r_e = 10.0 μm and r_e = 50.0 μm. As previously done in the clear-sky case, first, in order to account for model biases, the differences of the simulation and actual must be calculated. Then, the total differences of these calculations are computed to account for both model sensitivity and water vapor sensitivity. Finally, by taking the differences between the cloud-free date and the cloudy date, a total difference plot displays spectral features that can highlight where the water vapor continuum is dominant. Figure 11a displays the total differences between the cloud-free cloudy simulations and the cloud-cloudy simulations, and is representative of the contribution due to water vapor. A zoomed-in figure 11b highlights the same difference peaks as seen in Figure 10b. The greatest deviations are indicative of where the continuum is the predominant absorber. Like *Delamere et al*., 2010, Figure 10b shows that the five microwindows that may need updates are centered at 410, 477, 497, 533, and 560 cm^{-1}. Figure 11b also suggests some continuum absorption at 363 and 391 cm^{-1}. Future research should focus on updating the water vapor absorption continuum at these specific bands.

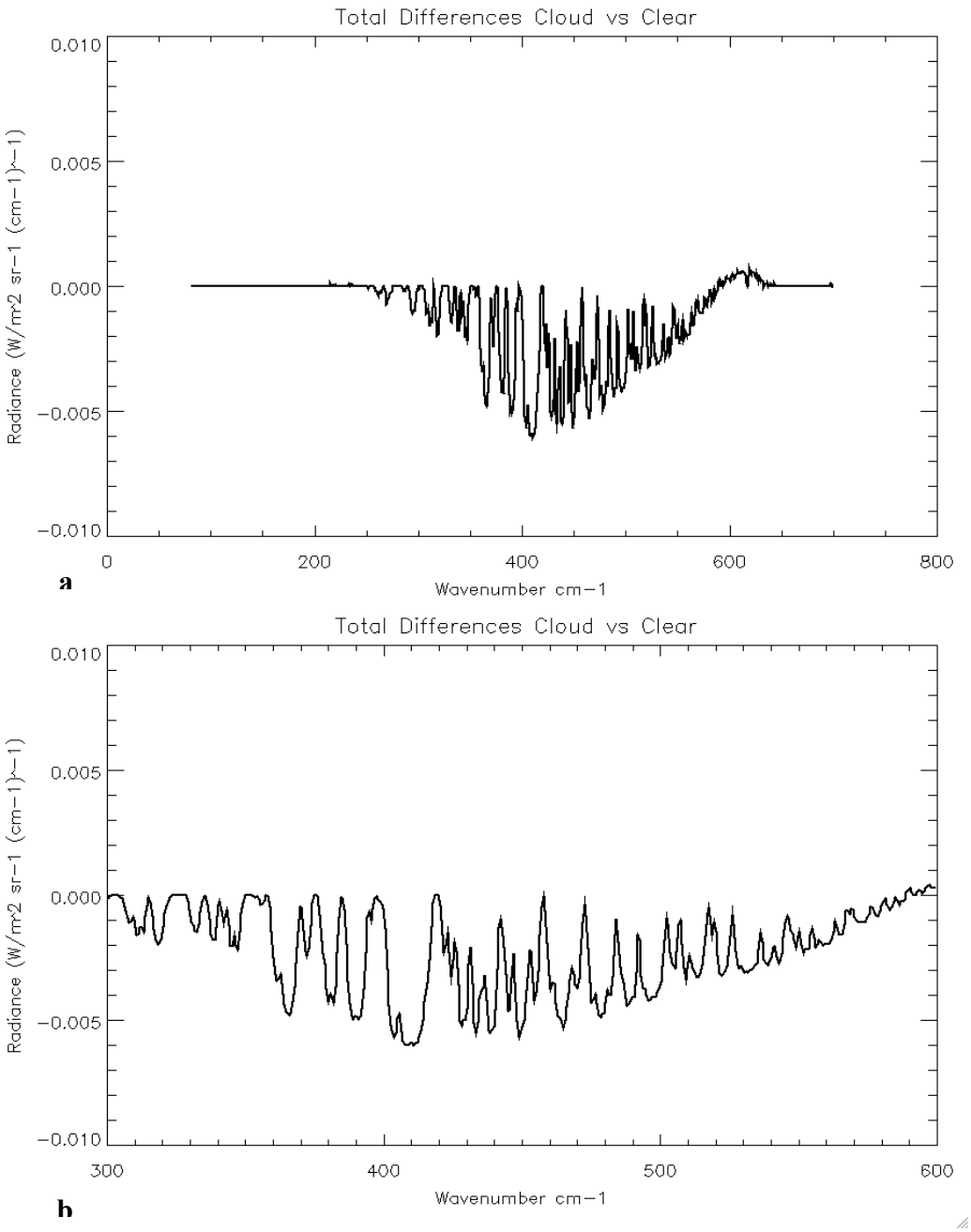

Figure 11: a.) The total differences between the cloud-free date cloudy simulation differences (13 September 2009 13:44z) and the cloud-cloudy simulation differences (01 October 2009, 17:40z) of different effective radius. b.) Spectral features between 300 and 600 cm^{-1} indicates bands where the continuum is the predominant absorber.

4.2.2 Optical Thickness Study

Next, to analyze the effect of changing optical thicknesses on this cloudy scenario, the same method used for evaluating effective size is applied. To be consistent all parameters will stay the same (cloud height = 6.13 km, effective radius = 10.0μm and solid column scattering database) while optical thickness is varied between 0.1 and 2.0, at visible wavelengths. Figure 12a depicts the differences between FIRST downwelling radiance measurements and the cloudy-model simulation if the optical thickness was τ = 2.0 (thick). Model calculations tend to be very sensitive at wavenumbers >380 cm^{-1} where the errors become as large as (-) 7.0 %. Note that errors are large because they are not representative of the cloud at this time. Errors bars are only used for spectral comparisons. In Figure 12b, when the optical thickness is τ = 1.0, we see slightly less error ((-) 4.0 %) at wavenumbers > 400 cm^{-1}. Finally Figure 12c shows that at very thin optical thicknesses (when τ < 0.3), the sensitivity is rather constant across the spectrum, with its greatest sensitivity peaks between 500 and 600 cm^{-1}. Peak to peak differences do not exceed +/- 0.07 % in radiance, except at the center of the CO_2 band at 667 cm^{-1} where absorption is large. Thus, optical thickness sensitivity tends to dominate the larger far-IR wavenumbers between 400 and 600 cm^{-1}, where scattering effects are greatest.

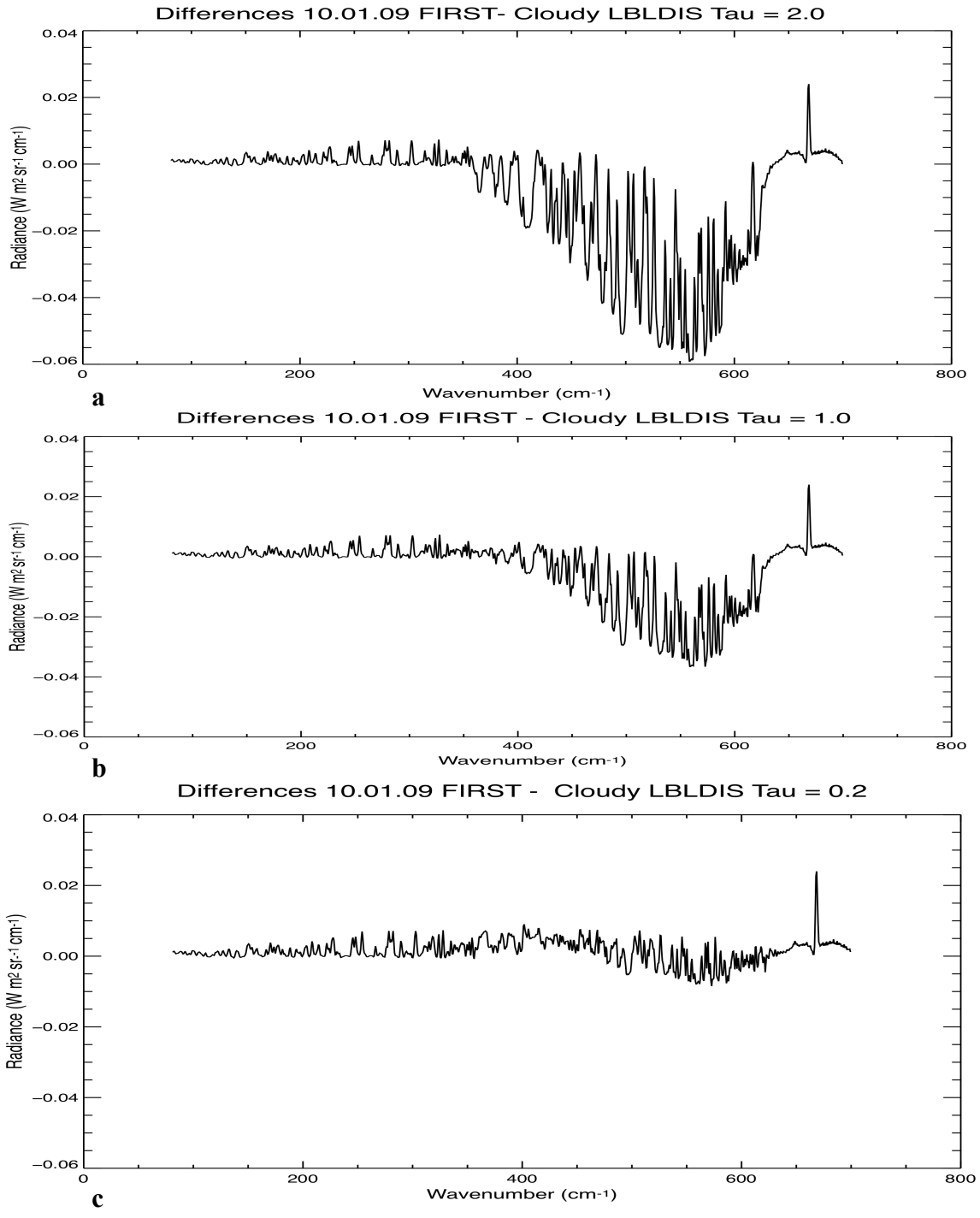

Figure 12: Downwelling radiance differences between FIRST measurements and model under a cloudy-sky simulation with constant cloud parameters, r_e = 10.0 μm and varying optical thickness values of (a) $\tau = 2$ (b) $\tau = 1$ and (c) $\tau = 0.2$.

In general for both cloud properties, optical thickness and effective radius, the model sensitivity up to 400 cm^{-1} is minimal, and is slightly more sensitive at larger wavenumbers > 400 cm^{-1}. Testing different size particles proved the water vapor continuum can account for some of the biases in the model simulations and should be updated in future work.

4.3 Using Brightness Temperature Differences to Determine Microphysical Cloud Properties

The prevalence of cirrus clouds is an important influence on climate change. To investigate the spectral radiative signature of ice clouds in the far-IR region, downwelling brightness temperatures are calculated. As previously discussed, optical thickness of clear-sky atmospheres at each layer are computed with the LBL radiative transfer model (*Clough et al.,* 1992) and are then passed to LBLDIS (*Turner,* 2005), along with the absorption properties to simulate cloudy sky downwelling radiances. The cloud temperature is assumed to be the same as the atmospheric temperature at that level and the surface is assumed to be a blackbody (unit emissivity 1). These radiances are used in the Planck function to calculate brightness temperature. Figure 13a displays brightness temperature calculations for cloudy sky simulations with different optical thickness. For optically thin clouds, scattering is strongest between 400-600 cm^{-1} and the amount of downwelling radiation is similar to a clear sky. As the clouds thicken, brightness temperatures warm due to the increasing absorptive properties of a thicker cloud layer and downwelling radiation increases, shown in Figure 13b.

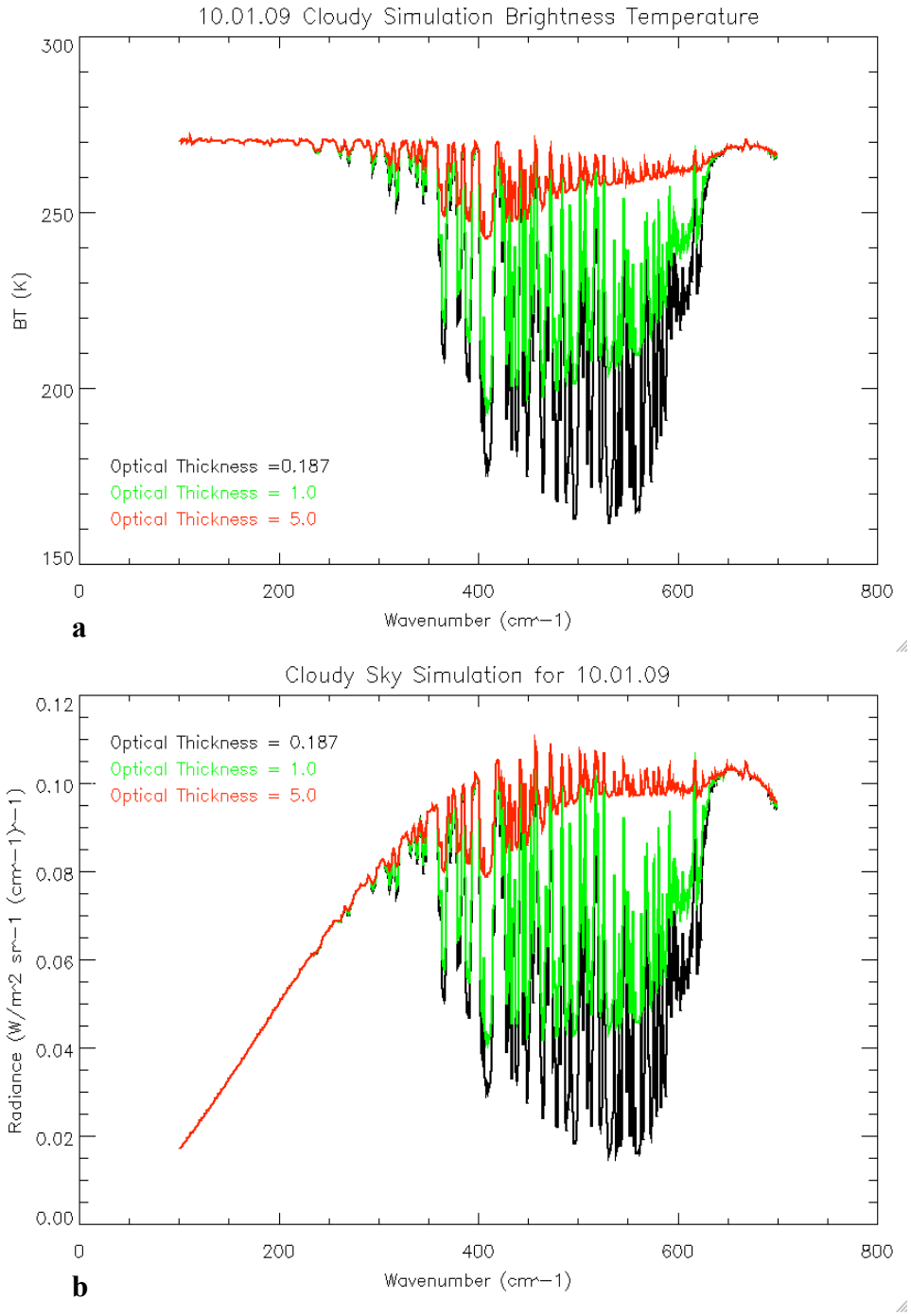

Figure 13: a.) Calculated downwelling brightness temperatures for cloudy sky simulations with varying optical thicknesses and r_e = 10.0 µm held constant. b.) Downwelling radiance for cloudy sky simulations under the same scenario. Scattering of particles largely influences the far-IR radiation between 400 and 600 cm^{-1} wavenumbers.

Yang et al., [2003] showed that optical depth can be inferred independent of cirrus particle size by calculating the brightness temperature differences between 250 and 559.5 wavenumbers (BTD 250-559.5 cm^{-1}). These channels are selected because one is located at a strong water vapor absorption band (250 cm^{-1}) and the other is located in an atmospheric transparent window (559.5 cm^{-1}). Brightness temperature is known to be inversely proportional to optical thickness, and thus allows for the properties of thin cirrus to be inferred. Results show that for a thin cirrus case, the brightness temperature difference is very low and close to -45K, whereas a thick cirrus cloud has a brightness temperature differences around -5K.

By using the inverse Planck function to calculate BTD 250-559.5 cm^{-1} of the measured FIRST data for 1 October 2009 17:40z, we find that the optical thickness is no greater than 0.023 (or 43K BTD) and a thin cirrus can be assumed. Table 3 displays BTD 250-559.5cm^{-1} for various optical thicknesses, identical to *Yang et al.,* [2003] findings. When optical thickness varies from 0.187 to 1.0, brightness temperature changes nearly 14K. At larger optical thicknesses, the brightness temperature differences saturate because of the strong absorption by ice particles. This implies that for ice clouds having small optical thicknesses the optical thickness may be inferred using far-IR data.

Table 3: Sensitivity of downwelling BTD 250-559.5cm^{-1} to various optical thicknesses with r_e=10.0 μm. BTD 250-559.5 cm^{-1} shows sensitivity to thin cirrus clouds and can potentially be used to infer optical thickness.

τ (tau)	**BTD 250-559.5cm^{-1} (K)**
τ =0.187 Thin	43.0
τ =0.5	36.9
τ =1.0	28.8
τ =5.0 Thick	6.3

4.4 Aerosol Study

To begin simulating aerosols in the far-IR, the DISORT model inputs are set for optical thickness of the aerosol plume (τ =1), and the layer at which the plume is located (layer 3 or 6.8 km (480 mb)). To get a general understanding of what occurs with a dust particle plume, Figure 14 displays the FIRST downwelling radiance measurements with the aerosol model simulation for the same date at the same spectral resolution. The aerosol simulation mimics the same spectral features as the FIRST measurements; noticeably the water vapor absorption bands (water vapor continuum) and the $C0_2$ absorption band at 667 cm-^{1}. The aerosol simulation also shows a reduction in downwelling radiance by almost one-half the clear-sky FIRST measurement. This follows the hygroscopic property of aerosols and their ability to attract and absorb water vapor.

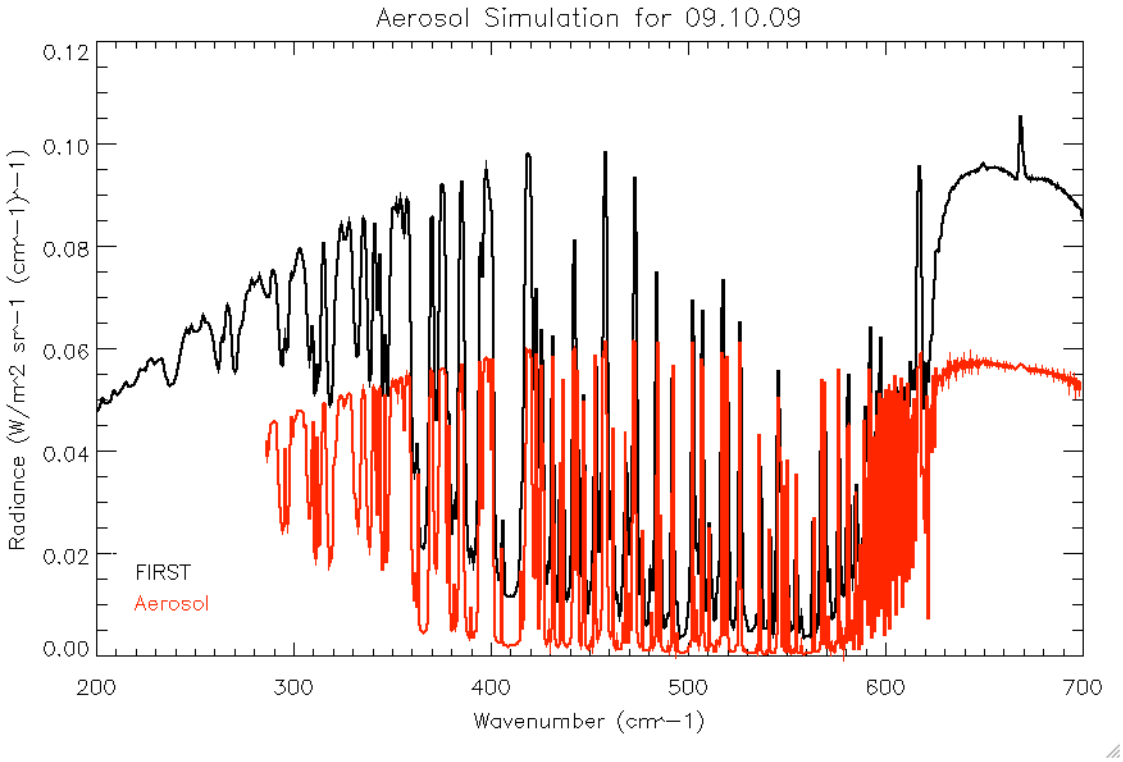

Figure 14: Aerosol simulation and FIRST downwelling radiance for 09 September 2009 at 15:29z.

However, to really understand the radiative forcing influence the aerosols are having on the far-IR, the same simulation must be done for the FIRST data with no aerosols in the same DISORT model. Figure 15 presents the difference between the 10 September 2009 15:29z, non-aerosol simulation and aerosol simulation both calculated using the DISORT model. By averaging the radiative forcing (RF) differences across the spectrum, the mean RF for this aerosol influence = 0.00235 W/m^2. To check for similarity, the same process was repeated for the date 03 October 2009 17:30z, and the mean RF was = 0.00129 W/m^2. If these dates are classified by moisture content, with

10 September 2009 (PWV = 0.5) exemplifying the dry case, and 03 October 2009 (PWV = 0.95) acting as the moist case, one can conclude that the aerosols had a greater influence on the far-IR spectrum during dry atmospheric conditions. However, the aerosol radiative effect may not be a significant contribution to radiative forcing in the far-IR.

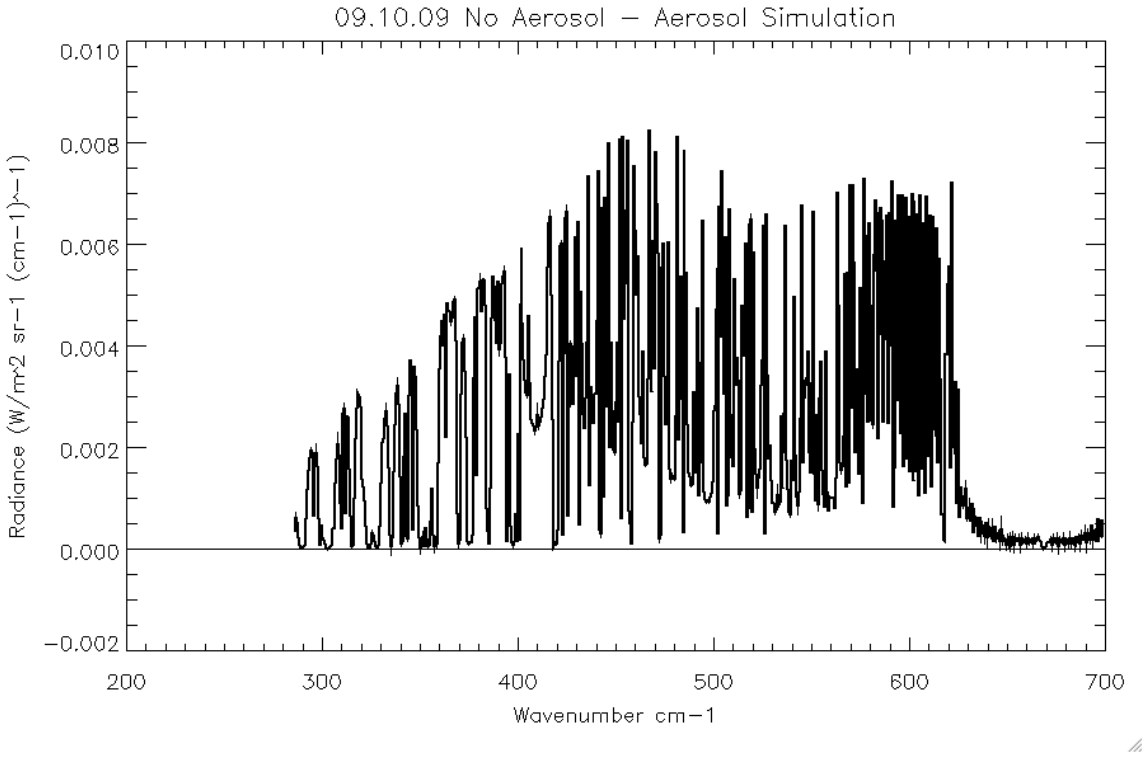

Figure 15: Calculated downwelling differences of a non-aerosol simulation and aerosol simulation for 10 September 2009 15:29z.

To understanding the differences of the water vapor content, it is worthy to compare a moist and dry day simulation for absorption strengths. Figure 16 displays the aerosol simulations for each respective case and day. For both the dry and moist aerosol cases, the absorption peaks and dips follow the same spectral features.

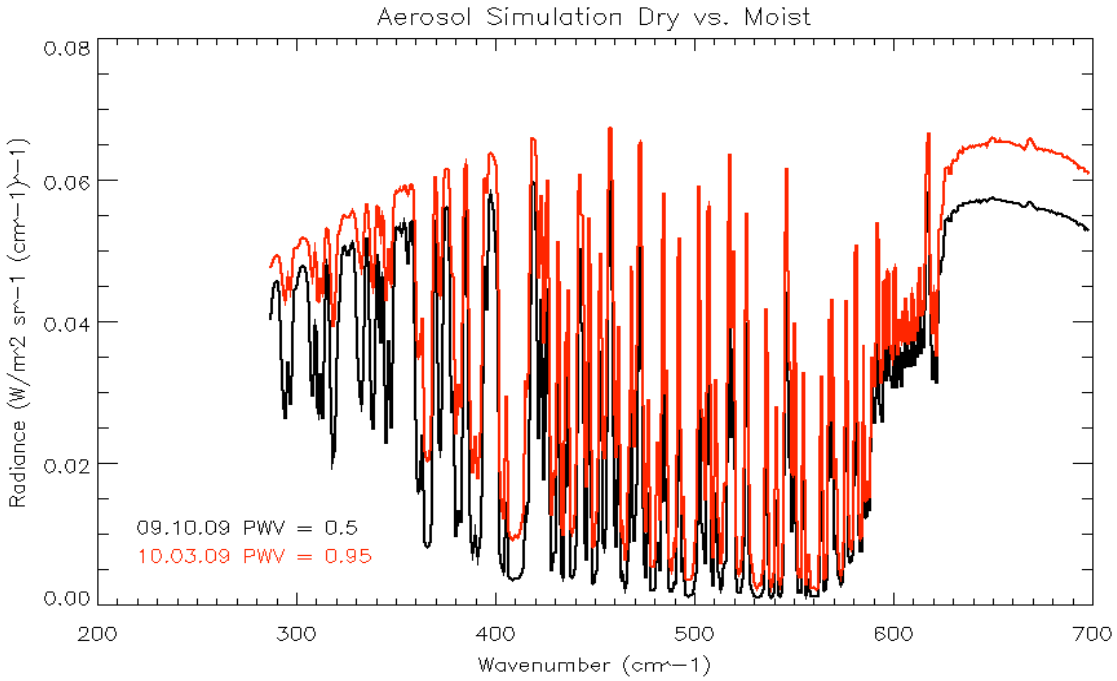

Figure 16: Dry and moist day comparisons of downwelling radiance for aerosol simulations in the far-IR.

To highlight possible water vapor continuum model absorption bands, the same process used in the cloudy sky simulations is repeated. First, the differences of each dates respected actual values (non-aerosol FIRST) and the aerosol simulation are calculated. Then the total differences between the dry and moist cases are calculated to highlight possible water vapor absorption bands. Figure 17 displays the total differences

of the two moisture cases and can be representative of where strong water vapor absorption bands may be.

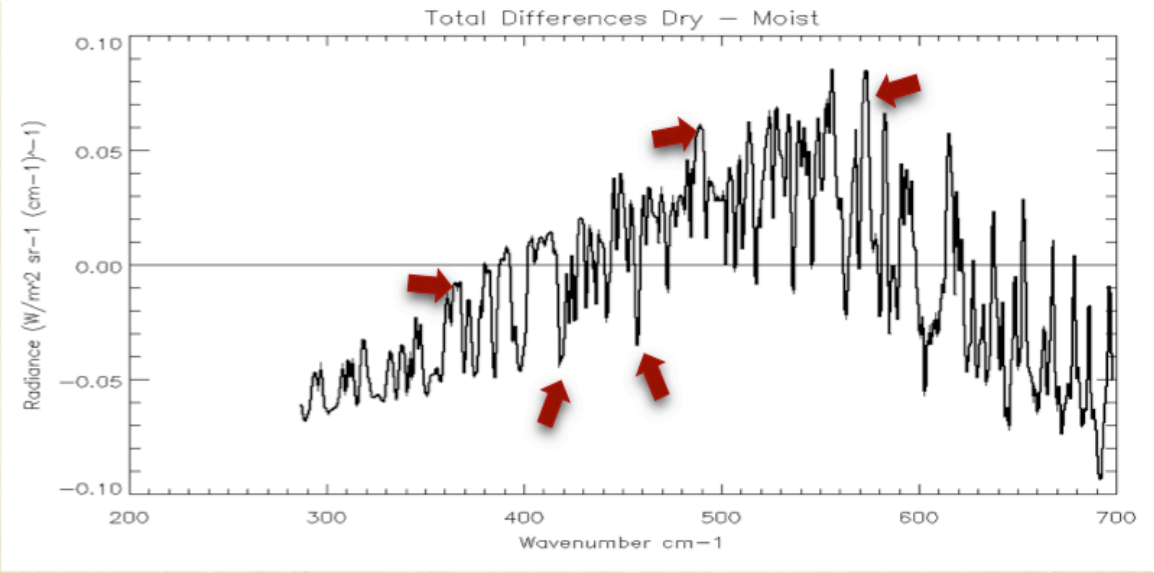

Figure 17: Differences of the dry and moist aerosol simulations can help to highlight where in the spectrum water vapor absorption bands are strong and where they may need future updates in the water vapor continuum.

It is evident in Figure 17 that some suggested absorption bands are near 360, 410, 470,490,560 and 600 cm^{-1}, which also match the bands that were presented in the cloudy-sky study. These absorption bands suggested may imply where the continuum model may need future updates.

5. SUMMARY AND CONCLUSIONS

There is strong agreement between the measured far-IR data set from Cerro Toco and the LBLDIS radiative transfer model when matching line shape and spectral resolution provided simultaneous sonde measured water vapor profiles. For both clear sky and cloudy sky simulations, peak to peak differences are very small and do not exceed +/- 0.7%, proving the models' consistency when used for hyperspectral far-IR analysis. These results show that cold, dry atmospheric profiles, such as Cerro Toco, tend toward surface radiances that are quite sensitive to model inputs. In particular the model is sensitive to moisture inputs at wavenumbers between 300 and 500 cm^{-1}. Using simultaneously acquired atmospheric profile variables (pressure, temperature, and relative humidity) is strongly recommended when comparing data with models calculating downwelling radiance in the far-IR. It is necessary to keep in mind that the bias in these analyses can be the combination of three errors: 1) the water vapor differences 2) the water vapor continuum model and 3) unknown instrument calibration error.

To distinguish if the water vapor continuum is the main culprit to these differences, difference analyses were done for both a dry date and a moist date, and for both clear and cloudy sky conditions. The total differences are representative of the contribution due to water vapor and the greatest deviations are indicative of where the continuum is the predominant absorber. Results highlighted that the five microwindows that are primary water vapor absorbers are centered at 410, 477, 497, 533, and 560 cm^{-1}, with additional suggestions at 363 and 391 cm^{-1}. These results are consistent with

Delamere et al., 2010. Future research should focus on updating the water vapor absorption continuum at these specific bands.

In addition to the clear sky simulations, cloudy sky simulations were also analyzed to determine the effects that the cloud microphysical properties, optical thickness and effective radius have in the far-IR. The cloud parameter particle effective radius has minimal effects on the model across the entire far-IR spectrum and indicated the need for more research on the water vapor absorption continuum model between 300 and 600 cm^{-1}. Conversely, the cloud parameter optical thickness has greater effects on the far-IR and tends to dominate at wavenumbers > 400 cm^{-1}, where the scattering effects of ice particles are greatest. Cloud parameters such as optical thickness are thus sensitive in the region where scattering dominates (> 400 cm^{-1}), while atmospheric conditions (moisture profile) are more sensitive in the region where absorption dominates (< 400 cm^{-1}).

Cloud optical thickness also proves to be consistent with previous studies and can be predicted from the difference in brightness temperature at wavenumbers 250 and 559.5 cm^{-1} [*Yang et al*., 2003]. These bands are used because one channel is located in a strong absorption band and the other is in a region of weak absorption, which is sensitive to the presence of ice clouds. The BTD 250 – 559.5 cm^{-1} proves effective when determining optical thickness for optically thin clouds using far-IR data.

Finally, the hygroscopic properties of aerosols are evident in the spectrum of the far-IR. When testing a basic tri-axial ellipsoid dust plume in the model, spectral features proved to again follow the pure rotational structure of water vapor. This spectral

structure for a third time highlighted the same primary water vapor absorption bands that the clear and cloudy sky analysis proved, reinforcing their importance for continuum updates. Additionally, aerosols acted to reduce the amount of downwelling radiation in the far-IR and absorbed about half of what would be emitted under a clear-sky. Despite this effect, aerosols may not have a significant contribution to the far-IR radiative forcing.

Together, to have the most optimal model for far-IR simulations, all input variables must be as accurate as possible. The far-IR is very sensitive to its surrounding atmospheric properties and cloud conditions. Developing proper algorithms for both cloud scene satellite collection and cloud scene data analysis will help to validate cloud data acquisition and lead to better understanding of the radiometric and microphysical properties in the far-IR. Future effort towards updating the water vapor absorption continuum in the far-IR at strong absorption bands can help to eliminate some of the cloud property biases of radiative transfer models in the far-IR. Effort regarding the comparison between the observations and simulations under cloudy conditions and continuum model updates is currently ongoing.

REFERENCES

Ackerman, S. A., R. E. Holz, R. Frey, E. W. Eloranta, B. C. Maddux, and M. McGill (2008), Cloud detection with MODIS. Part II: Validation, *J. Atmos. Oceanic Technol., 25*(7), 1073-1086, doi: 10.1175/2007JTECHA1053.1.

Baran, A. J. (2005), The dependence of cirrus infrared radiative properties on ice crystal geometry and shape of the size-distribution function, *Q. J. R. Meteorol. Soc., 131*(607), 1129-1142, doi: 10.1256/qj.04.91.

Baum, B. A., P. Yang, S. Nasiri, A. K. Heidinger, A. Heymsfield, and J. Li (2007), Bulk scattering properties for the remote sensing of ice clouds. Part III: High-resolution spectral models from 100 to 3250 cm−1, *J. Appl. Meteor. Climatol., 46*(4), 423-434, doi: 10.1175/JAM2473.1.

Cageao, R., A. Alford, D. Johnson, D. Kratz, and M. Mlynczak (2010), Far-IR measurements at Cerro Toco, Chile: FIRST, REFIR, and AERI, *Proc. SPIE 7808*, 78080T, DOI:10.1117/12.862601

Clough, S. A., M. J. Iacono and J.L. Moncet, (1992), Line-by-line calculation of atmospheric fluxes and cooling rates: Application to water vapor, *J. Geophys. Res., 97,* 15761-15785.

Clough, S., P. Brown, N. Miller, J. Liljegren, and T. Shippert (1994), Residual analysis of surface spectral radiances between instrument observations and line-by-line calculations, *Proceedings of the Fourth Atmospheric Radiation Measurement (ARM) science team meeting*, 101-109, CONF-940277, U.S. Department of Energy, Washington, D.C.

Clough, S. A., M. W. Shephard, E. J. Mlawer, J. S. Delamere, M. J. Iacono, K. Cady-Pereira, S. Boukabara, and P. D. Brown (2005) Atmospheric radiative transfer modeling: a summary of the AER codes, Short Communication, *J. Quant. Spectrosc. Radiat.Transfer, 91*, 233-244.

Collins, W. D. and M. G. Mlynczak (2001). Prospects for measurement of far-infrared tropospheric spectra: implications for climate modeling, Paper GC32A-0210, Fall AGU Meeting 2001, San Francisco, CA.

Cox, C. V., J. E. Harries, J. P. Taylor, P. D. Green, A. J. Baran, J. C. Pickering, A. E. Last, and J. E. Murray (2010), Measurement and simulation of mid- and far-infrared spectra in the presence of cirrus, *Quarterly Journal of the Royal Meteorological Society*, *136*, 718-739 doi: 10.1002/qj.596.

Delamere, J. S., S. A. Clough, V. H. Payne, E. J. Mlawer, D. D. Turner, and R. R. Gamache (2010), A far-infrared radiative closure study in the Arctic: Application to water vapor, *J. Geophys. Res., 115*, D17106, doi:10.1029/2009JD012968

Fleming, J. R. and S. K. Cox (1974), Radiative effects of cirrus clouds, *J. Atmos. Sci., 31(*8), 2182-2188, doi: 10.1175/1520-0469

Foot, J. S. (1988), Some observations of the optical properties of clouds: II Cirrus, *Quarterly Journal of the Royal Meteorological Society, 114*, 145–164.

Harries, J., B. Carli, R. Rizzi, C. Serio, M. Mlynczak, L. Palchetti, T. Maestri, H. Brindley, and G. Masiello (2008), The Far-infrared Earth*, Rev. Geophys., 46*, RG4004, doi:10.1029/2007RG000233.

Heymsfield, A. J., S. Lewis, A. Bansemer, J. Iaquinta, L. M. Miloshevich, M. Kajikawa, C. Twohy, and M. R. Poellot (2002), A General Approach for Deriving the Properties of Cirrus and Stratiform Ice Cloud Particles, *J. Atmos. Sci., 59*(1), 3-29, doi: 10.1175/1520-0469

Key, J. R. (2002), Parameterization of shortwave ice cloud optical properties for various particle habits, *Journal of Geophysical Research, 107*(D13), 4181 doi:10.1029/2001JD000742.

Lee, Y., P. Yang, M. I. Mishchenko, B. A. Baum, Y. X. Hu, H. Huang, W. J. Wiscombe, and A. J. Baran (2003), Use of circular cylinders as surrogates for hexagonal pristine ice crystals in scattering calculations at infrared wavelengths, *Appl. Opt., 42*(15), 2653, doi: 10.1364/AO.42.002653.

Levoni, C., M. Cervino, R. Guzzi, and F. Torricella (1997). Atmospheric aerosol optical properties: a database of radiative characteristics for different components and classes. *Applied Optics, 36*(30), 8031–8041.

Liou, K. (1986), Influence of cirrus clouds on weather and climate processes: A global perspective, *Mon. Wea. Rev., 114*(6), 1167-1199, doi: 10.1175/1520-0493

Lynch DK, K. Sassen, D.O. Starr, G. Stephens (Eds.), *Cirrus*, Oxford Univ. Press, New York, 2002.

McFarquhar, G. M., A. J. Heymsfield, A. Macke, J. Iaquinta, and S. M. Aulenbach (1999), Use of observed ice crystal sizes and shapes to calculate mean-

scattering properties and multispectral radiances: CEPEX April 4, 1993, case study, *Journal of Geophysical Research, 104*(D24), 31763-31779, doi: 10.1029/1999JD900802.

Meng, Z., P. Yang, G. W. Kattawar, L. Bi, K. N. Liou, I. Laszlo, 2010: Single-scattering Properties of Nonspherical Mineral Dust Aerosols: A Database for Application to Radiative Transfer Calculations, *J. of Aerosol Science*, *41*, 501-512.

Meyer, K., P. Yang, and B. Gao, (2004), Optical thickness of tropical cirrus clouds derived from the MODIS 0.66and 1.375-μm channels, Geoscience and Remote Sensing, *IEEE Transactions of Geosci , 42,* 4, pp. 833-841.doi:10.1109/TGRS.2003.818939

Miloshevich, L., H. Vomel, D. Whiteman, and T. Leblanc (2009), Accuracy assessment and correction of vaisala RS92 radiosonde water vapor measurements, *J. Geophysical. Research*, *B*, doi:10.1029/2008JD011565.

Mlynczak, M.G., D. Johnson, G. Bingham, K. Jucks, W. Traub, L. Gordley and P. Yang (2005), The far-infrared spectroscopy of the troposphere (FIRST) project, *Proc. SPIE 5659, 81*; doi:10.1117/12.579063

Mlynczak M.G., D. Johnson, H. Latvakoski, K. Jucks, M. Watson et al. (2006), First light from the Far-Infrared Spectroscopy of the Troposphere (FIRST) instrument, *Geophys. Res. Lett*. 33, L07704, doi:10.1029/2005GL025114.

Rothman, L. S., D. Jacquemart, A. Barbe, D. Benner, L. Brown et al. (2005), The HITRAN 2004 molecular spectroscopic database, *Journal of Quantitative Spectroscopy and Radiative Transfer*, *96*(2), 139-204, doi: DOI:

10.1016/j.jqsrt.2004.10.008.

Seemann, S. W., E. E. Borbas, R. O. Knuteson, G. R. Stephenson, and H. Huang (2008), Development of a global infrared land surface emissivity database for application to clear sky sounding retrievals from multispectral satellite radiance measurements, *J. Appl. Meteor. Climatol.*, 47(1), 108-123, doi: 10.1175/2007JAMC1590.1.

Stamnes, K., S. Tsay, W. Wiscombe, and K. Jayaweera (1988), A numerically stable algorithm for discrete-ordinate-method radiative transfer in multiple scattering and emitting layered media*, Appl. Opt.,27*(12), 2502-2509, doi: 10.1364/AO.27.002502.

Turner, D.D., S. A. Ackerman, B. A. Baum, H. E. Revercomb, and P. Yang (2003), Cloud phase determination using ground-based AERI observations at SHEBA, *J. Appl. Meteor*., *42*, 701–715.

Turner, D.D. (2005), Arctic mixed-phase cloud properties from AERI-lidar observations: algorithm and results from SHEBA, *J. Appl. Meteor*., *44*, 427-444, doi:10.1175/JAM2208.1.

Turner, D. D. and E. J. Mlawer (2010), The Radiative Heating in Underexplored Bands campaigns, *Bull. Amer. Meteor. Soc*., *91*, 911–923. doi: 10.1175/2010BAMS2904.1

Warren, S. G. (1984), Optical constants of ice from the ultraviolet to the microwave, *Appl. Opt*., *23*(8), 1206, doi: 10.1364/AO.23.001206.

Wiscombe, W. J. (1980), Improved mie scattering algorithms, *Appl. Opt*., *19*(9), 1505,

doi: 10.1364/AO.19.001505.

Yang, P., K.N.,Liou (1996a), Geometric-optics-integral-equation method for light scattering by nonspherical ice crystals, *Appl. Opt., 35*, 6568-6584.

Yang, P., K.N. Liou (1996b), Finite-difference time domain method for light scattering by small ice crystals in three-dimensional space, *Journal of the Optical Society of America A.*, *13*(10), 2072, doi: 10.1364/JOSAA.13.002072.

Yang, P., M. G. Mlynczak, H. Wei, D. P. Kratz, B. A. Baum, Y. X. Hu, W. J. Wiscombe, A. Heidinger,and M. Mischenko (2003), Spectral signature of ice clouds in the far-infrared region: Single scattering calculations and radiative sensitivity study, *J. Geophys., Res., 108*, 4569, doi:0.1029/2002JD003291.

Yang, P., H. Wei, H. L Huang, B. A. Baum, Y. X. Hu, M. I. Mishchenko, and Q. Fu (2005), Scattering and absorption property database of various nonspherical ice particles in the infrared and far-infrared spectral region. *Appl. Opt., 44*, 5512-5523

VITA

Name:	Elizabeth Ann Baugher
Address:	Department of Atmospheric Sciences Texas A&M University 3150 TAMU College Station, TX 77843-3150
Email Address:	eab5076@tamu.edu
Education:	B.S., Meteorology, Penn State University, 2009 M.S., Atmospheric Sciences, Texas A&M University, 2011